Miner Petrol (2017) 111:291–314
DOI 10.1007/s00710-016-0472-0

ORIGINAL PAPER

The growth and contamination mechanism of the Cana Brava layered mafic-ultramafic complex: new field and geochemical evidences

Tommaso Giovanardi[1] · **Vicente A. V. Girardi**[1] · **Ciro T. Correia**[1] · **Silvano Sinigoi**[2] · **Colombo C. G. Tassinari**[1] · **Maurizio Mazzucchelli**[3]

Received: 18 January 2016 / Accepted: 13 September 2016 / Published online: 22 September 2016

Abstract The Cana Brava complex is the northernmost of three layered complexes outcropping in the Goiás state (central Brasil). New field and geochemical evidences suggest that Cana Brava underwent hyper- to subsolidus deformation during its growth, acquiring a high-temperature foliation that is generally interpreted as the result of a granulite-facies metamorphic event. The increase along the stratigraphy of the incompatible elements abundances (LREE, Rb, Ba) and of the Sr isotopic composition, coupled with a decrease in $\varepsilon Nd_{(790)}$, indicate that the complex was contaminated by the embedded xenoliths from the Palmeirópolis Sequence. The geochemical data suggest that the contamination occurred along the entire magma column during the crystallization of the Upper Mafic Zone, with in situ variations determined by the abundance and composition of the xenoliths. These features of the Cana Brava complex point to an extremely similarity with the Lower Sequence of the most known Niquelândia intrusion (the central of the three complexes). This, together with the evidences that the two complexes have the same age (c.a. 790 Ma) and their thickness and units decrease northwards suggests that Cana Brava and Niquelândia are part of a single giant Brasilia body grown through several melt impulses.

Keywords Mafic complex · Goiás · Cana Brava · Niquelândia · Geochemistry

Editorial handling: F. Gervilla

Electronic supplementary material The online version of this article (doi:10.1007/s00710-016-0472-0) contains supplementary material, which is available to authorized users.

✉ Tommaso Giovanardi
tommaso.giovanardi@gmail.com

[1] Instituto de Geociências, Universidade de São Paulo, Rua do Lago, 562, Cidade Universitária, São Paulo 05508-900, Brazil

[2] Dipartimento di Geoscienze, Università degli Studi di Trieste, Via E.Weiss, 8, I-34128 Trieste, Italy

[3] Dipartimento di Scienze Chimiche e Geologiche, Università di Modena e Reggio Emilia, Via Campi, 103, I-41125 Modena, Italy

Introduction

The Cana Brava mafic-ultramafic complex is the northernmost of three large layered complexes that form a discontinuous, 300 km long, North-trending belt within the Brasilia Belt (Goiás state, central Brasil) (Girardi et al. 1978; Correia et al. 1997; Correia and Girardi 1998; Ferreira Filho et al. 2010). The three complexes (from South to North: Barro Alto, Niquelândia and Cana Brava) are elongated parallel to the Maranhão thrust belt, a major tectonic boundary formed during the Brazilian (Panafrican, ~600 Ma) collision of the Amazonian and São Francisco cratons (Pimentel et al. 2000). A large positive gravimetric anomaly overlaps the alignment of the complexes suggesting that the three complexes may be tectonically separated fragments of a single body, tilted and uplifted during the Brazilian event (Feininger et al. 1991; Marangoni et al. 1995; Ferreira Filho et al. 2010; Correia et al. 2012). Among the three layered complexes, Niquelândia is the best studied (Rivalenti et al. 1982, 2008; Girardi et al. 1986; Pimentel et al. 2004a, 2006; Correia et al. 2007, 2012), whereas Barro Alto and Cana Brava are less known (Matsui et al. 1976; Girardi et al. 1978; Fugi 1989; Suita et al. 1994; Correia et al. 1997, 1999; Correia and Girardi 1998; Moraes and Fuck 2000; Ferreira Filho et al. 2010; Della Giustina et al. 2011; Giovanardi et al. 2015).

The magmatic textures of the rocks of the three complexes are obliterated by a super-imposed foliation parallel to their alignment and direction. This foliation is intepreted as metamorphic, according to the observation that the complexes

were re-crystallized in granulite- to amphibolite-facies (Pimentel et al. 2004b; Ferreira Filho et al. 2010; and references therein). Conversely, Correia et al. (2012) re-interpreted structural, textural and chemical features of the Niquelândia complex, providing evidences that its intrusion occurred through significant shear under hyper- to sub-solidus conditions during the growth and cooling of a crystal mush. Their U-Pb SHRIMP zircons data constrain the Niquelândia intrusion at ~790 Ma (Rivalenti et al. 2008; Correia et al. 2012), an age similar to those reported by Ferreira Filho et al. (2010) and Giovanardi et al. (2015) for the Cana Brava intrusion. Correia et al. (2012) report also a detailed study of the contamination of the Niquelândia complex, due to the assimilation of xenoliths from the upper metavolcanic-metasedimentary sequence (the Indaianopólis Sequence). In a previous study, Correia et al. (1997) suggest that also the Cana Brava complex was affected by crustal contamination; however, no details about the contamination are reported.

In this paper, we present new geochemical data of the Cana Brava complex and a comparison with literature data, as well as structural observations, of Niquelândia. The data are discussed in order to: i) constrain the occurrence of the contamination process during the growth of the Cana Brava complex, ii) evaluate the style of the contamination process, iii) discuss the evidences of metamorphism versus syn-magmatic deformation, and iv) discuss the possibility that Cana Brava and Niquelândia are separated fragments of one giant layered complex.

Geological setting

The Cana Brava layered complex

The Cana Brava layered complex is about 40 km long with a 10°-20° NNE main strike and 30°-50° dip (Fig. 1; Correia and Girardi 1998). Its estimated thickness decreases progressively from about 12 km in the southern side, vanishing to the North. To the East, the Cana Brava complex overthrusts the Rio Maranhão Thrust Zone (formed by thrust of rocks of different regional units such as the Serra da Mesa Group, the Araí Group and the Araxá Group). The western contact of the complex is intrusive in the metasediments and metavolcanics of the Palmeirópolis Sequence (Ribeiro Filho and Teixeira 1981; Girardi and Kurat 1982; Correia et al. 1997; Correia and Girardi 1998). The igneous nature of the western contact is consistent with the absence of mylonites near the contact (Correia and Girardi 1998) and with the occurrence of xenoliths from the Palmeirópolis Sequence (SP) within the upper levels of the Cana Brava complex (Correia et al. 1997; Correia and Girardi 1998; Giovanardi et al. 2015). To the South and North the complex is bounded by normal and strike-slip faults (Fig. 1).

Correia et al. (1997) and Correia and Girardi (1998) divided the Cana Brava complex in five units, however, in this study, we will use the simpler subdivision in three units based on the lithological criteria proposed by Ferreira Filho et al. (2010). From the lower unit (East) to the top (West), the complex consists of:

i) A Lower Mafic Zone (LMZ) mainly formed by epidote-bearing amphibolites and interlayered gabbros commonly with mylonitic texture. Rare porphyroclastic textures and pyroxenes partially substituted by amphibole (Tremolite-Actinolite) are recognized (Correia and Girardi 1998). Correia and Girardi (1998) suggest that the mylonitic texture and the pyroxenes and plagioclase substitution are a consequence of pervasive fluid percolation within this unit during the tectonic emplacement of the Cana Brava complex.

ii) An Ultramafic Zone (UZ) mainly of meta-peridotites with locally interlayered meta-pyroxenites. Serpentinites and amphibolites are the result of fluid-assisted low-grade metamorphism and hydrothermal processes, which affected dunites, peridotites and pyroxenite layers (Dreher et al. 1989; Correia et al. 1997; Correia and Girardi 1998; see Biondi 2014, for a detailed study). Locally, it is possible to recognize the primary cumulus texture. The top of the unit consists mainly of cumulate websterite (orthopyroxene between 15 and 25 %, clinopyroxene between 75 and 85 %). Approaching the top of the websterite layer, a gradational modal increase of orthopyroxene and plagioclase and a decrease of clinopyroxene are observed (Correia and Girardi 1998). Plagioclase is generally interstitial. Pyroxenes are sometimes replaced by amphibole and biotite (Correia and Girardi 1998). The transition to the Upper Mafic Zone is gradational with an increase of gabbro layers approaching the boundary. The thickness of the UZ is around 1.9 km in the southern part of the body and decreases progressively northwards. In the northern part, the UZ locally disappears, in a sort of boudinage. The websterite layer at the roof of the UZ has a thickness of ~500 m in the southern part of the complex and tends to disappear northward (Fig. 1).

iii) An Upper Mafic Zone (UMZ) mainly consisting of gabbros, gabbronorites and norites, with subordinate diorites, quartz-rich gabbros, quartz-rich diorites and, locally, tonalites mostly near the complex roof (Correia and Girardi 1998). The rocks commonly show igneous textures overprinted locally by a high temperature foliation, defined by the orientation of orthopyroxene, clinopyroxene and plagioclase (Correia and Girardi 1998). Minor/accessories phases are quartz, biotite, amphibole, spinel, apatite, titanite, rutile and zircon. Epidote and calcite are secondary phases. Approaching

the roof of the complex, the rocks of the UMZ show an increase in biotite, amphibole and quartz and a decrease in orthopyroxene and clinopyroxene.

The contact with the stratigraphic upper Palmeirópolis Sequence is magmatic (Girardi and Kurat 1982; Correia and Girardi 1998). Xenoliths of the rocks of the Palmeirópolis Sequence are common in this unit, especially in the proximity of the roof, and may occur as both isolated fragments or layers parallel to the foliation. In the southern and central part of the Cana Brava complex, the majority of the crustal xenoliths are amphibolites, whereas quartzite levels have been observed in the northern part (Correia et al. 1997; Correia and Girardi 1998).

The Palmeirópolis Sequence is the most extended (c.a. 80 km long and up to 35 km wide) among the metavolcanic-metasedimentary sequences in contact with the Goiás layered complexes (the others are the Juscelândia Sequence at Barro Alto and the Indaianopólis at Niquelândia). The Palmeirópolis, Indaianopólis and Juscelândia sequences share similar stratigraphy and lithologies (Ferreira Filho et al. 2010 and references therein). These sequences mainly consist of metasediments (i.e. metacherts, metapelites and calc-silicate rocks) with interbedded amphibolites, gneisses and intrusive and sub-volcanic granites with typical MORB-like affinity (Brod and Jost 1991; Araújo et al. 1995; Araújo 1996; Moraes and Fuck 1994, 1999; Moraes et al. 2003, 2006; Ferreira Filho et al. 2010). The metavolcanics have both E-MORB and N-MORB affinities and this bi-modal volcanism has been ascribed to a transitional setting from a continental rift to an oceanic basin (Araújo 1996; Moraes et al. 2003, 2006). The rocks show metamorphic recrystallization, from amphibolite-facies, near the contacts with the complexes, to greenschist-facies (Araújo 1996; Moraes et al. 2003, 2006; Ferreira Filho et al. 2010 and references therein). Local granulite-facies conditions were also reported (Ferreira Filho et al. 2010 and references therein).

Comparison of Cana Brava and Niquelândia stratigraphy

The Niquelândia layered complex is the best known among the three Goiás layered complexes. It is about 40 km long and

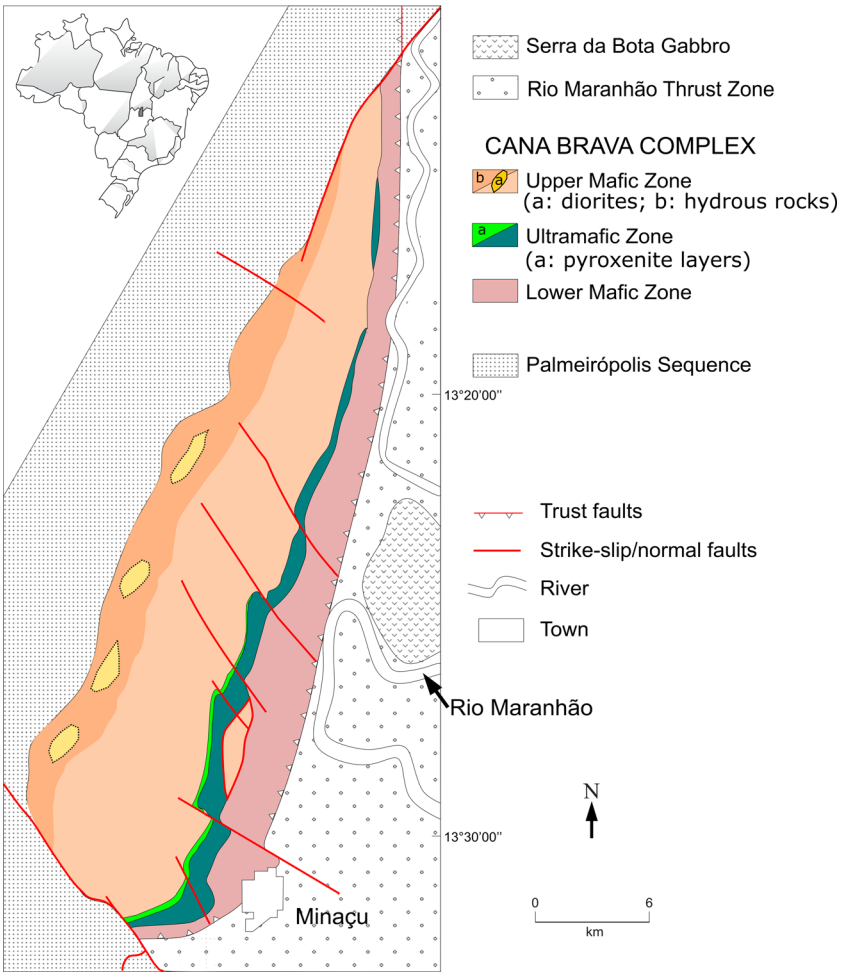

Fig. 1 Geological map of the Cana Brava complex, modified from Correia et al. (1997) and Ferreira Filho et al. (2010)

20 km wide and lies in tectonic contact with the rocks of the Rio Maranhão Thrust Zone to the E and in magmatic contact with the highest stratigraphic portion of the metavolcanic-metasedimentary sequence of Indaianopólis to the W (Correia et al. 2012 and references therein). The stratigraphy of the Niquelândia complex has been defined in various ways (see Ferreira Filho et al. 2010 and Correia et al. 2012). According to Correia et al. (2012), we divide the Niquelândia complex in two main sequences: the Lower Sequence (LS) and the Upper Sequence (US).

The LS is similar to the Cana Brava complex. From the E to the W it is formed by:

1) The Basal Gabbro Zone (BGZ), formed by gabbros interlayered with pyroxenites and peridotites. These rocks are commonly recrystallized by tectonic deformation, and correspond to the LMZ of the Cana Brava complex.
2) The Basal Peridotite Zone (BPZ) formed by massive cumulus dunites and harzburgites.
3) The Lower Ultramafic Zone (LUZ) formed by interlayered pyroxenites and peridotites with subordinate gabbros. The entire unit of BPZ and LUZ corresponds to the UZ of Cana Brava.
4) The Layered Gabbro Zone (LGZ) mainly formed by gabbros, gabbronorites and norites with subordinate biotite- and amphibole-gabbros, quartz-diorites and, locally, tonalites near the roof (the so-called 'Hydrous Zone', HZ). In this unit, bands and swarms of xenoliths of the same lithotypes from the upper portion of the Indaianopólis Sequence also occur. This unit corresponds to the UMZ of Cana Brava.

The US is divided in two units: the Upper Gabbro-Anorthosite Zone (UGAZ) and the Upper Amphibolite (UA):

5) The UGAZ is formed by olivine-gabbros, gabbros and anorthosites.
6) The UA mainly represents the magmatic, gradational contact between the Niquelândia complex and the Indaianopólis Sequence. This unit is formed by the alternation of amphibole-gabbro (considered as part of the complex) and garnet-bearing amphibolite (considered as part of the metavolcanic-metasedimentary sequence, which is similar to the Palmeirópolis Sequence).

A comparison of the Niquelândia and Cana Brava stratigraphy reveals that the US rocks are missing in the Cana Brava complex. The estimated thickness of the whole Niquelândia complex is c.a. 18 km. The estimated thicknesses, considering direction and dip, of the Niquelândia LS and the Cana Brava complex in its southern part (c.a. 12 km) are similar.

Age of the intrusion

Several intrusion ages of the Cana Brava complex have been published in the literature. Matsui et al. (1976) provided two Ar-Ar whole-rock isochrones on gabbros, norites and amphibolites of 1935 ± 110 Ma and 475 ± 15 Ma and several K-Ar ages distributed over a wide time span from 3950 Ma to 480 Ma. Girardi et al. (1978) dated two gneisses from the Palmeirópolis Sequence and the Serra da Mesa Group with Rb-Sr whole-rock isochrones at 1157 ± 150 Ma and 644 ± 27 Ma, respectively. They interpreted these ages as two distinct metamorphic events, which recrystallized the gneisses under amphibolite facies.

Fugi (1989) provided a Sm-Nd whole-rock isochron for the Cana Brava complex at 1970 ± 69 Ma, interpreted as the intrusion age. Correia et al. (1997) reported a Rb-Sr whole-rock isochron and an internal Sm-Nd isochron (plagioclase + biotite + pyroxene), which yielded ages of 1350 ± 35 Ma and 770 ± 43 Ma, respectively. They calculated the regression of the Sr isotopes evolution curve of the Cana Brava complex, obtaining a minimum age for mantle differentiation at 2250 Ma, interpreted as the time of the Cana Brava intrusion, whereas the younger isochron ages (i.e. 1350 ± 35 Ma and 770 ± 43 Ma) were attributed to two different metamorphic events.

The large age range given by whole rock "isochrones" is likely an artefact of the variability of the initial isotopic ratios of these largely contaminated rocks, as proposed by Ferreira Filho et al. (2010). Contamination processes are well known for the Niquelândia complex (Correia et al. 2007, 2012; Rivalenti et al. 2008) and have also affected the Cana Brava complex, as shown in this paper. In such circumstances, the best methodology to obtain reliable ages is by U-Pb zircon geochronology. Ferreira Filho et al. (2010) determined U-Pb TIMS zircon ages at 782 ± 3 Ma and 779 ± 1 Ma on two samples from the UMZ and UZ (four and three analyses, respectively) and interpreted them as the intrusion age of the Cana Brava complex. U-Pb SHRIMP-II analyses on zircons from 4 samples of the Cana Brava complex (from the UMZ) reported by Giovanardi et al. (2015) provided concordia ages between 791.9 ± 9.0 Ma and 778.0 ± 6.7 Ma, consistent with those obtained by Ferreira Filho et al. (2010).

Post igneous evolution of the Cana Brava complex

Girardi and Kurat (1982), Correia et al. (1997), Correia and Girardi (1998), Ferreira Filho et al. (2010) and Biondi (2014) recognized that several metamorphic episodes have affected the Cana Brava complex. According to Correia et al. (1997), a first metamorphic event was responsible for the re-equilibration of pyroxenes and plagioclase under granulite-facies conditions at about 900 °C and 6–7 kbar. However, Girardi and Kurat (1982) and Correia and Girardi (1998)

suggested that this recrystallization "event" could be the consequence of the slow cooling of the Cana Brava complex. In contrast, Ferreira Filho et al. (2010) and Biondi (2014) documented a later granulite-facies event, which would have occurred around 770–760 Ma. According to all, the first metamorphic event caused the penetrative, high-temperature foliation and lineation of the rocks, a re-orientation of the igneous layering and the formation of mylonites and shear zones. Moreover, Correia et al. (1997) proposed that the tectonic transport of the Cana Brava complex occurred during this phase. The second metamorphic event proposed by Girardi and Kurat (1982) and Correia et al. (1997) occurred in upper-amphibolite facies as the retrograde event related to the first metamorphic peak (i.e. the granulite-facies metamorphism). During a late reactivation of faults and shear zones, hydrous fluids migrated from the deformed area through the complex and produced the substitution of pyroxenes by amphibole (Girardi and Kurat 1982; Correia et al. 1997).

The last metamorphic event occurred as a low-grade episode under hydrothermal conditions, with fluids introduction in the lower units of the Cana Brava complex (i.e. the LMZ and UZ) and the formation of serpentinites, low-grade amphibolites and rodingites (Girardi and Kurat 1982; Dreher et al. 1989; Girardi et al. 1991; Correia and Girardi 1998; Ferreira Filho et al. 2010; Biondi 2014). According to Correia and Girardi (1998), Ferreira Filho et al. (2010) and Biondi (2014), this event was concurrent to the exhumation and the overthrust of the Cana Brava complex above the Serra da Mesa Group at 630 Ma, during the continental collision between the São Francisco and Amazonian cratons.

Field observations

A recent study of the Niquelândia complex re-interpreted the structural features and provided new evidences suggesting that the deformation of the complex occurred during its growth under hyper- to sub-solidus conditions (Correia et al. 2012). New field studies were conducted in the Cana Brava area to provide new constraints on the dispute about metamorphic vs syn-magmatic deformation. These field works were also performed in order to better define the nature of the western contact of the complex and the relationship between the Cana Brava complex and the Palmeirópolis Sequence.

The websterite layer at the roof of the UZ is about 500 m thick in the southern sector of the Cana Brava complex (Correia and Girardi 1998). In the central sector, it grades in a < 10 m thick swarm of thin layers (mm-to-cm, Fig. 2a) of pyroxenite interfingered with gabbro. This layered package is locally anastomosed and vanishes to the north. The layering is parallel to the foliation, and both are locally cut by undeformed gabbro or pyroxenite dykes (Fig. 2a). Some of these undeformed dykes crosscut a boulder at the base of UMZ in the central sector of the complex formed by foliated gabbro in contact with a major felsic domain (Fig. 2b) and late swarms of felsic veins and layers in the UMZ gabbros (Fig. 2c).

Most igneous rocks of both Cana Brava and Niquelândia are affected by granoblastic re-crystallization and high-T foliation parallel to the modal banding. These features were interpreted by various authors as evidences of a granulite-facies metamorphic event (Ferreira Filho et al. 1992, 1998; Ferreira Filho and Pimentel 2000). However, Correia et al. (2012) observed that, in Niquelândia, the high-T foliation is locally cut by undeformed veins of leuco-gabbro (Fig. 3), as commonly found in other large mafic intrusions (e.g., Ivrea-Verbano, Quick et al. 1992, 1994).

Similar structures are also present in Cana Brava (Fig. 2), providing evidences for melt percolation after the development of the foliation. This leads to conclude that, rather than evidence of a later granulite-facies metamorphic event, the high-T foliation is the result of hyper-solidus shear, which affected a largely crystallized crystal mush during the growth of the igneous body. The stretching that caused the high-T foliation may also be responsible, at least in part, for the progressive thinning northwards of the entire igneous complex.

In general, the abundance of hydrous phases increases approaching the top of the Cana Brava complex; however, it is not constant along the roof, showing a heterogeneous distribution. Their maximum amount is recognized in patches of amphibole- and biotite-rich, locally garnet-bearing diorites, which in general contain abundant xenoliths (amphibolites) from the Palmeirópolis Sequence (Fig. 4a). The xenoliths are rimmed by a micro-gabbro chilled margin (Fig. 4b). Banding is parallel to a high-T foliation defined by iso-orientation of plagioclase, biotite ± amphibole (Fig. 4b).

The dimension of the Palmeirópolis Sequence xenoliths seems to decrease from the base to the top of the UMZ. At the deepest levels of the UMZ, crustal inclusions are mainly quartzite layers of big size (cm-to-m thick and hundreds of meters long, elongated parallel to the foliation), which are predominant in the northern sector of the complex. At higher levels, in the central UMZ, the xenoliths are mainly separated fragments (rarely longer than 1 m). Locally, crustal xenoliths from the Palmeirópolis Sequence are surrounded by undeformed leucosome, which may eventually fill the pressure shadow of pseudo-boudinage structures, suggesting that the xenoliths were partially molten during the shear that caused the foliation (Figs. 4c, d). Frequently, the xenoliths are elongated parallel to the foliation, as observed in the "Hydrous Zone" in Niquelândia (Figs. 3 and 4).

In the central and upper parts of UMZ, the xenoliths are mainly garnet-bearing amphibolite and amphibolite. Subordinate xenoliths of quartzites and garnet-bearing schists rich in biotite occur approaching the complex roof.

Similar rocks are common in the lower Palmeirópolis Sequence near and at the contact with the Cana Brava complex (Figueiredo et al. 1981). Minor quartzite, metachert and iron banded layers are intercalated within the amphibolites (Figueiredo et al. 1981), and are similar to the quartzite septa included in the lower UMZ (Correia and Girardi 1998; this study). The similarities between xenoliths and rocks of the complex suggest that, if not from the Palmeirópolis Sequence, the xenoliths derived from an extremely similar metavolcanic-metasedimentary sequence.

Analytical methods

A total of 34 new samples from the Cana Brava complex were analysed for bulk rock major and trace elements to integrate the dataset of Correia and Girardi (1998) and to compare the geochemical variations of Cana Brava and Niquelândia. Ten of these samples were selected for mineral chemistry (for both major and trace elements) and their petrography is reported in Online Resource A.

Major element bulk rock analyses were performed by X-ray fluorescence, using a wavelength dispersive Philips PW 2400 spectrometry, using fused glass disks according to procedures described by Mori et al. (1999). Accuracy was greater than 2 %. Trace element analyses in selected samples were performed by Inductively Coupled Plasma-Mass Spectrometry (ICP-MS) using the procedure described by Navarro et al. (2008). Accuracy, determined with respect to the reference standards BHVO-2 and BR, was 0.5–2 %. Data are reported in Online Resource B.

On selected samples, Sm-Nd and Rb-Sr isotopic determination were carried out by Isotope Dilution Thermal Ionization Mass Spectrometry (ID-TIMS), following the procedure described in Sato et al. (1995). The isotopic ratios of the studied samples were measured on a VG Iso-mass 354 automated mass spectrometer using five Faraday collectors in static mode. Data are reported in Table 1. The $^{143}Nd/^{144}Nd$ ratio was corrected to standard JNdi-1 (Tanaka et al. 2000) with a reference value $^{143}Nd/^{144}Nd = 0.512097$ (± 0.000009, $n = 23$). The $^{87}Sr/^{86}Sr$ ratio was corrected to standard NBS-987 (Moore et al. 1982) with a reference value $^{87}Sr/^{86}Sr = 0.710235$ (± 0.000025 between March and April 2015).

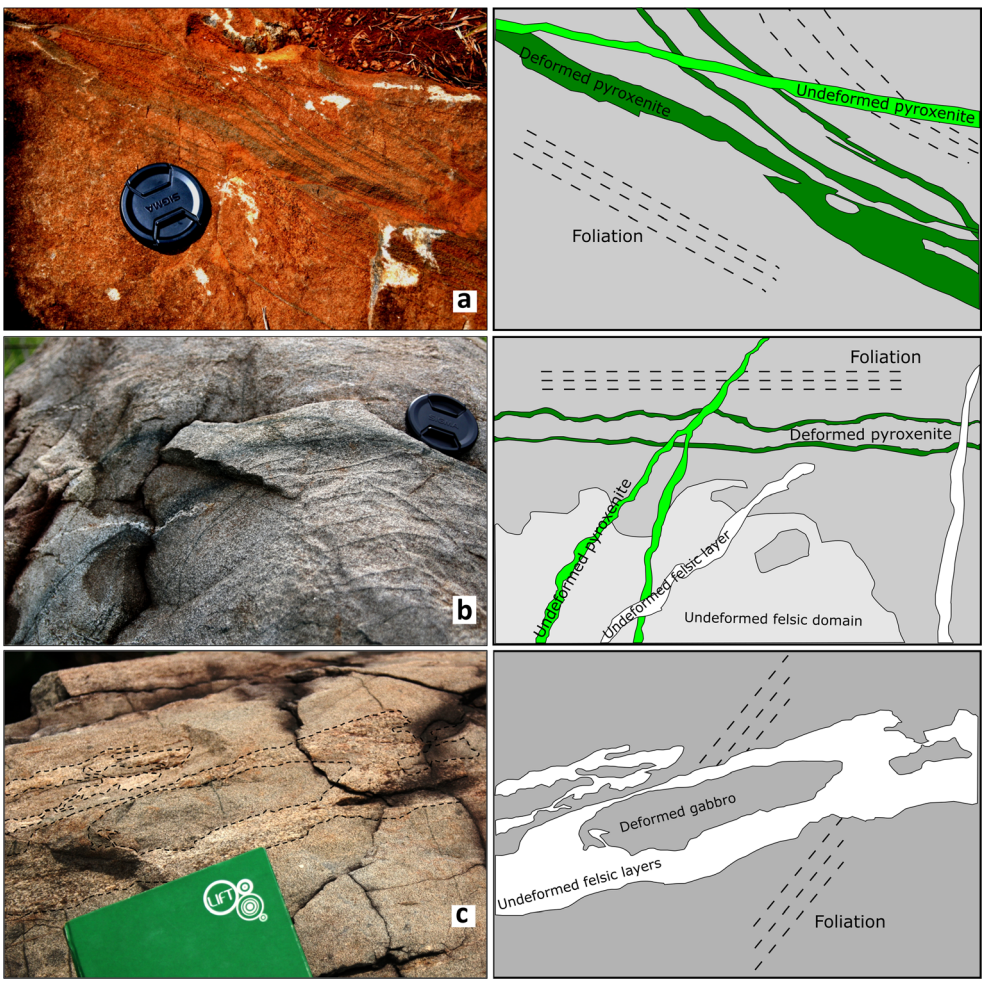

Fig. 2 Selected images of the field relationships from the Cana Brava complex: **a** deformed websterite layers in the northern part of the Cana Brava complex crosscutted by late undeformed vein; **b** gabbro of the lower UMZ in contact with a felsic domain crosscutted by pyroxenites and anorthositic veins; **c** late felsic veins parallel to the gabbro foliation. A schematic sketch of the major features of each picture is also presented

Major element in mineral were analysed by Electron Probe Micro Analyses (EMPA) with a JEOL 8200 Super Probe (data are reported in Online Resource C) after thin section carbon coating. Analytical conditions were 15 kV of acceleration voltage, 15 nA of primary current beam, 10 s counting time for each element and 5 s counting time for the background. Data were checked and corrected using cation mass balance with different O normalization for each phases (Amphibole and Biotite: 23 O; pyroxenes: 6 O and 4 cations p.f.u.; Titanite: 5 O and 3 cations p.f.u.; Ilmenite: 3 O and 2 cations p.f.u.; Garnet: 12 O and 8 cations p.f.u.; Plagioclase: 8 O and 5 cations p.f.u.; Fe_T as Fe^{2+}). Average analyses of the mineral phases are reported in Table 2 and full analyses are reported in Online Resource C.

Trace elements spot analyses on the same samples were determined by Laser ablation-inductively coupled plasma-mass spectrometry (LA-ICP-MS), using a ThermoFisher Scientific Mass Spectrometer coupled to a laser ablation New Wave UP 213. Data reduction was achieved with the Thermo Fisher Scientific PlasmaLab® software using NIST610, NIST612 and NIST614 as external standards. The isotope ^{44}Ca was used as internal standard for Amphibole, Clinopyroxene, Plagioclase and Garnet and ^{29}Si for Biotite and Quartz. Laser spot size was calibrated at 80 μm and laser beam fluency at 20 microJoule for cm^2. Data are reported in Online Resource C.

Quartz internal structures of the quartzite sample CB1425 were observed by CathodoLuminescence (CL) images obtained during EMPA analytical sessions by JEOL 8200 Super Probe and a CL-C detector (JEOL). Analytical conditions were: high voltage =15 kV, work distance =11 mm, detector = PMT, filament emission =15 nA, and magnification range = 40 to 65 × .

Results

Chemical variations vs stratigraphy

In Figs. 5, 6 and 7 we present plots of the chemical variations vs. stratigraphy of the most significant trace elements for Cana Brava (this paper and Correia and Girardi 1998) and the lower Niquelândia (Correia et al. 2012). Given that the upper Niquelândia sector has a different stratigraphy when compared to Cana Brava, we disregard it in this comparison.

The most prominent feature is a sudden increase in incompatible elements abundances (K, Rb, Ba, and others) in the uppermost 2 km of the section approaching the roof of Cana Brava. Similar features are also observed in the "Hydrous Zone" of Niquelândia (Rivalenti et al. 2008; Correia et al. 2012; Fig. 7). In addition, an increase in the scattering of $(La/Yb)_N$ up section is observed. This ratio, which is roughly indicative of the REE pattern, reaches the highest values at levels where xenoliths are particularly abundant, especially in the proximity of the roof and on a specific level at about 8 km from the bottom of the sequence.

The K_2O, Ba, Rb and La abundances are constant throughout the UMZ, with local enrichments between 6 and 8 km and a strong enrichment at the roof of the complex. The K_2O content ranges between 0.03–0.44 wt% in the UMZ and between 0.09–2.62 wt% at the roof (Figs. 5 and 6). The Ba content varies between 8 and 142 ppm in the UMZ and between 11 and 1760 ppm in the uppermost 2 km. The Rb content varies between 0.4–74 ppm in the UMZ and between 1.3–105 ppm at the roof of the complex. The La content varies between 1 and 24 ppm in the UMZ and between 6 and 40 ppm in the uppermost 2 km.

Fig. 3 Selected images of field textures from the Niquelândia complex: **a** late undeformed pyroxenite vein crosscutting the superimposed foliation; **b** undeformed gabbroic layers crosscutting the foliation and a deformed pyroxenite layer; **c** deformed xenoliths parallel to the gabbro foliation in the LGZ; **d** xenolith aligned to the gabbro foliation in the LGZ

Moderately incompatible elements such as Sr, Nd and Y show two distinct enrichment peaks, the first in the central UMZ (corresponding to the 6–8 km level) and the second at the roof of the complex (Fig. 5). The Nb and Zr content shows a similar behaviour. In the central UMZ, Sr = 20–1124 ppm, Nd = 4–31.5 ppm, Y = 5–57 ppm, Nb = 2–91 ppm and Zr = 6–224 ppm, whereas at the roof of the complex Sr = 95–327 ppm, Nd = 7–47.4 ppm, Y = 7–91.3 ppm, Nb = 5–26 ppm and Zr = 23–605 ppm. The enrichment in incompatible elements approaching the roof of the complex is also shown by the REE patterns (Fig. 8). Samples from LMZ are slightly enriched in LREE and show flat trends for MREE and HREE (Fig. 8). Samples from UZ show depleted and flat trends consistent with cumulus of pyroxenes. Samples from UMZ show flat to slightly enriched LREE patterns (Fig. 8). Samples from the uppermost 2 km of the complex are enriched in LREE. Eu anomalies range from negative to positive (Fig. 8).

The $(La/Sm)_N$ ratio increases along the stratigraphy similarly to the $(La/Yb)_N$ ratio (Fig. 6). The highest variations occur between 6 and 8 km ($(La/Sm)_N$ = 1.19–2.74; $(La/Yb)_N$ = 1.25–4.90) and at the roof of the complex ($(La/Sm)_N$ = 2.38–4.03; $(La/Yb)_N$ = 2.53–17.98).

The spread and increase of incompatible and moderately incompatible elements approaching the complex roof is concomitant with the increase of hydrous phases and the maximum abundance of xenoliths within the complex. However, local enrichments are also present throughout the entire UMZ, in particular between 6 and 8 km (Figs. 5 and 6). These local enrichments occur in gabbros in contact/near xenoliths (sometimes clustered in levels).

Several amphibolites from the Palmeirópolis Sequence were analysed by Correia and Girardi (1998). Amphibolites show heterogeneous compositions, with some samples enriched in incompatible elements (e.g. Ba, Rb, Sr and Nd; Figs. 5 and 6): K_2O = 0.12–2.81 wt%, Ba =12–1711 ppm, Rb = 2–101 ppm, Sr = 9–1150 ppm, Nd = 9–38 ppm, Y = 12–54 ppm. Amphibolite compositional ranges are similar to those of xenoliths within the complex (Figs. 5 and 6) and only few xenoliths from the complex roof, which are representative of the subordinate quartzites and garnet-bearing schists, show higher values for K_2O, Nd and Y. The similar compositions of amphibolites from the Palmeirópolis Sequence and from xenoliths within the complex, suggest that the latter were rocks of the Palmeirópolis Sequence incorporated during the growth of the complex.

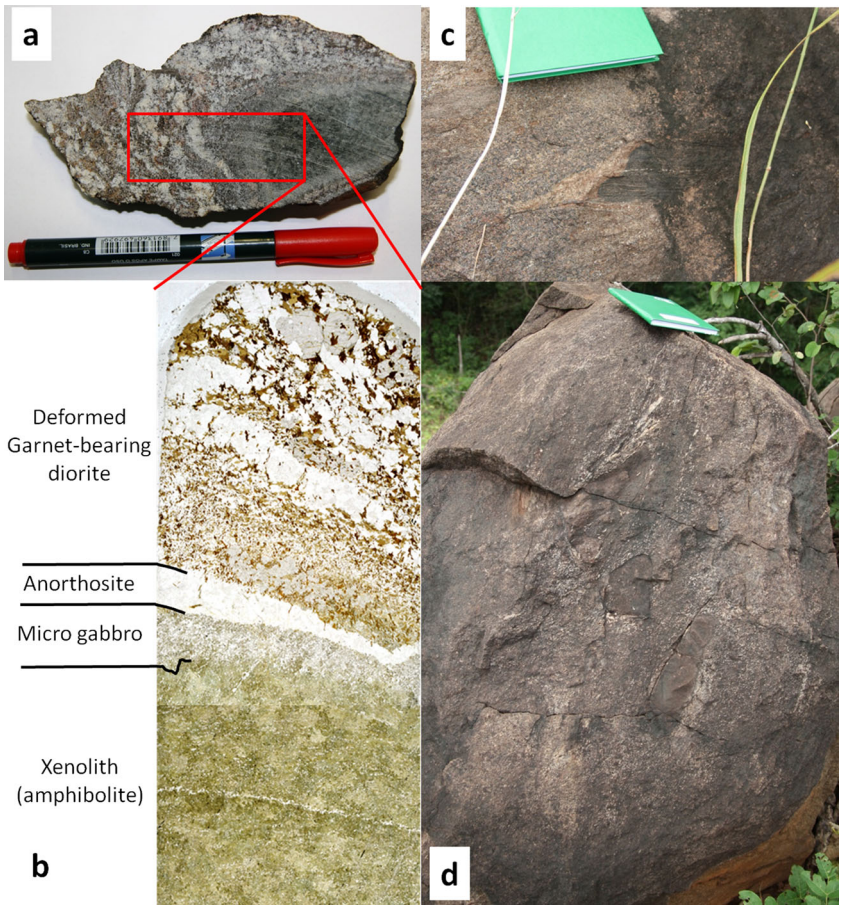

Fig. 4 Selected images of field relationships from the Cana Brava complex: **a** amphibolite xenolith in a garnet-bearing diorite of the roof complex; **b** section of the 4a xenolith and host diorite with highlighted areas of different composition; **c** deformed mafic enclaves and felsic 'pressure shadow' domain; **d** undeformed xenoliths aligned with the gabbro foliation and occurrence of late felsic domains along the deformation at the top of the complex

Sr and Nd isotopes

Table 1 reports Sr and Nd isotopic compositions determined on 10 new samples and 3 samples analysed by Correia et al. (1997). All isotopic ratios are recalculated at 790 Ma. Pyroxenite sample CB1133 has a $^{87}Sr/^{86}Sr_{(790)}$ ratio of 0.708243 (which is the lowest value within the Cana Brava sample collection) and an $\varepsilon Nd_{(790)}$ of −0.78 (Table 1; Fig. 9). Across the stratigraphy, the $^{87}Sr/^{86}Sr_{(790)}$ ratio shows a continuous increase approaching the roof of the complex (Table 1; Fig. 9), reaching a maximum value of 0.730470 in the Garnet-diorite sample (CB1482) and of 0.736590 in an Amphibole-bearing gabbro (sample CB1490). These values are higher than the two samples reported by Correia et al. (1997) at the roof of the complex ($^{87}Sr/^{86}Sr_{(790)}$ = 0.724609 and 0.725265), resulting in a large spread in $^{87}Sr/^{86}Sr_{(790)}$ in the uppermost 2 Km, similar to what is observed in LIL elements (Table 1; Figs. 5 and 9). Conversely, the $\varepsilon Nd_{(790)}$ trend decreases only moderately approaching the top, where it reaches values of −8.42 in the diorite sample and of −8.47 in the gabbro sample (Table 1; Fig. 9). Comparing $^{87}Sr/^{86}Sr_{(790)}$ and $\varepsilon Nd_{(790)}$ an inverse correlation between the two values is evident (Fig. 10). Only sample CB1434 deviates from this trend showing an $\varepsilon Nd_{(790)}$ value of 1.70, with a $^{87}Sr/^{86}Sr_{(790)}$ ratio (0.711978) (Table 1; Figs. 9 and 10).

The xenolith shows $^{87}Sr/^{86}Sr_{(790)}$ ratio and $\varepsilon Nd_{(790)}$ comparable with the gabbroic rocks (0.728076 and −8.01 respectively; Fig. 9). Conversely, the Palmeirópolis Sequence sample has a clear mantle signature, with $^{87}Sr/^{86}Sr_{(790)}$ = 0.703278 and $\varepsilon Nd_{(790)}$ = 12.81.

Mineral chemistry

Mafic phases in igneous rocks of Cana Brava are generally in equilibrium as shown by the good correlation trends for Mg# (R^2 between 0.95–0.98; Fig. 11). Mineral compositions along the stratigraphy vary according to bulk-rock variation (Online Resource D). Amphibole (classified as Pargasite, Pargasite-Edenite and Mg-Hornblende in the rocks of the complex) cores are enriched in TiO_2 and FeO relative to the rims, but are depleted in Al_2O_3 (Tab. 2). In amphibole, the CaO content is higher in the cores than in the rims in the rocks of the lowest statigraphic levels (between 0 and 6 km), whereas the opposite zoning is observed at the highest levels (Tab. 2). Along the UMZ stratigraphy, amphibole shows enrichments in TiO_2, FeO and CaO and depletion in Al_2O_3. The Na_2O and K_2O content shows depletion trend up to 8 km and enrichments approaching the complex roof. Similar trends are recognizable for clinopyroxene and orthopyroxene (except for K_2O, Tab. 2). Clinopyroxene cores are enriched in FeO and depleted in CaO (Tab. 2). Conversely, the orthopyroxene cores are enriched in CaO in rocks at stratigraphic levels underneath 8 km and became depleted afterwards (Tab. 2). Plagioclase

Table 1 Rb-Sr and Sm-Nd bulk-rock isotopic compositions by Isotopic Dilution Thermal Ionization Mass Spectrometry (ID-TIMS) for selected samples

Sample	Unit	Sm (ppm)	Nd (ppm)	$^{147}Sm/^{144}Nd$	$^{143}Nd/^{144}Nd$	2σ	$\varepsilon Nd_{(790)}$	Rb (ppm)	Sr (ppm)	$^{87}Rb/^{86}Sr$	2σ	$^{87}Sr/^{86}Sr$	2σ	$^{87}Sr/^{86}Sr_{(790)}$
CB1133	UZ	1.86	6.16	0.181402	0.512519	0.000009	-0.78	7.4	100	0.212365		0.710639	0.000064	0.708243
CB1434	UMZ	2.57	9.89	0.156308	0.512516	0.000008	1.70	0.723	153	0.013688		0.712132	0.000046	0.711978
CB1464	UMZ	0.932	2.87	0.195159	0.512341	0.000007	-5.65	0.396	122	0.009405		0.715977	0.000057	0.715871
CB1424	UMZ	1.66	5.75	0.174039	0.512225	0.000007	-5.78	0.439	233	0.005453		0.717050	0.000038	0.716988
CB1414	UMZ	1.87	6.37	0.176302	0.512181	0.000008	-6.87	0.569	114	0.014495		0.717464	0.000057	0.717300
CB1475	UMZ	3.39	12.5	0.163794	0.512187	0.000007	-5.48	0.639	182	0.010154		0.722621	0.000065	0.722506
CB1490	UMZ	7.98	37	0.128606	0.511852	0.000009	-8.47	1.33	169	0.022718		0.736846	0.000063	0.736590
CB1482	UMZ	2.19	10.5	0.125985	0.511841	0.000010	-8.42	40	204	0.571063		0.736912	0.000057	0.730470
CB1060	Xen UMZ	2.76	13.1	0.126365	0.511864	0.000007	-8.01	4.59	215	0.061859		0.728774	0.000070	0.728076
SP0003	PAL	4.08	14.0	0.175417	0.513183	0.000007	12.81	7.45	149	0.144361		0.704907	0.000063	0.703278
CB1006	LMZ							0.3	59.4	0.016	0.001	0.71772	0.00061	0.717540
CB1029	UMZ							75.5	209.4	1.047	0.021	0.73642	0.00022	0.724609
CB1099	UMZ							101.8	285.6	1.034	0.017	0.73693	0.00018	0.725265

The lower three lines quote Rb-Sr data of Correia et al. (1997)

Table 2 Compositions of rock-forming minerals (EPMA results, in wt%) originating from core and rim regions of each rock sample, respectively

Phase	Clinopyroxene average													
Sample	CB1042		CB1434		CB1464		CB1424		CB1414		CB1475		SP0003	
Unit	UZ		UMZ		UMZ		UMZ		UMZ		UMZ		SP	
Rock Type	websterite		gabbro		gabbro		diorite		gabbro		gabbro		amphibolite	
Strat Pos (m)	3514		4858		4874		7053		7456		8221		12000	
Position	core	rim	core	rim	core	rim	core	rim	core	rim	core	rim	core	rim
SiO_2	52.29	52.42	53.37	53.87	53.10	53.06	51.87	51.95	53.54	53.48	53.04	53.29	52.12	52.19
TiO_2	0.48	0.49	0.24	0.17	0.23	0.21	0.19	0.14	0.15	0.16	0.13	0.13	0.17	0.11
Al_2O_3	4.57	4.22	2.40	2.08	2.18	2.14	1.95	2.23	1.58	1.61	1.31	1.32	1.58	1.34
Cr_2O_3	1.05	1.07	0.12	0.08	0.16	0.22	0.01	0.03	0.35	0.30	0.03	0.03	0.01	0.02
FeO_T	2.36	2.15	6.81	5.55	7.06	7.16	11.80	11.32	6.54	6.07	8.29	7.74	12.00	11.61
MnO	0.07	0.10	0.15	0.14	0.21	0.21	0.35	0.29	0.20	0.17	0.25	0.22	0.37	0.40
NiO	0.04	0.03	0.03	0.02	0.03	0.01	0.01	0.01	0.01	0.02	0.03	0.01	0.03	0.01
MgO	15.64	15.67	15.73	16.06	13.91	13.80	11.55	11.68	15.24	15.16	13.96	14.03	10.82	11.03
CaO	22.74	23.05	20.45	21.53	22.83	22.81	21.74	21.95	22.19	22.69	22.44	22.94	22.80	23.02
Na_2O	0.75	0.73	0.60	0.56	0.50	0.52	0.39	0.44	0.38	0.37	0.34	0.35	0.34	0.30
K_2O	0.00	0.00	0.01	0.01	0.00	0.01	0.00	0.00	0.00	0.00	0.00	0.00	0.00	0.00
Mg#	0.92	0.93	0.81	0.84	0.78	0.77	0.64	0.65	0.81	0.82	0.75	0.76	0.62	0.63
Phase	Orthopyroxene average													
Sample	CB1042		CB1434		CB1464		CB1424		CB1414		CB1475		CB1482	
Unit	UZ		UMZ		UMZ		UMZ		UMZ		UMZ		UMZ	
Rock Type	websterite		gabbro		gabbro		diorite		gabbro		gabbro		Grt-diorite	
Strat Pos (m)	3514		4858		4874		7053		7456		8221		10557	
Position	core	rim	core	rim	core	rim	core	rim	core	rim	core	rim	core	rim
SiO_2	55.11	55.14	53.69	53.62	52.90	52.74	50.71	50.74	53.57	53.56	52.33	52.46	51.46	51.56
TiO_2	0.07	0.04	0.06	0.03	0.08	0.08	0.06	0.06	0.05	0.04	0.07	0.04	0.10	0.08
Al_2O_3	3.20	3.03	1.59	1.72	1.45	1.45	1.27	1.40	1.11	1.22	1.00	0.96	0.90	0.93
Cr_2O_3	0.54	0.53	0.02	0.05	0.09	0.06	0.02	0.02	0.16	0.12	0.03	0.02	0.01	0.01
FeO_T	8.67	8.74	18.68	18.41	22.08	22.20	30.18	30.07	20.01	20.05	24.60	24.80	28.64	28.61
MnO	0.18	0.18	0.40	0.41	0.46	0.47	0.84	0.80	0.45	0.45	0.54	0.54	0.31	0.28
NiO	0.06	0.07	0.06	0.01	0.01	0.01	0.02	0.03	0.02	0.01	0.01	0.01	0.01	0.02
MgO	31.72	31.83	25.05	25.17	22.59	22.56	16.50	16.46	24.11	24.18	20.96	20.79	17.94	17.90
CaO	0.34	0.22	0.36	0.32	0.52	0.37	0.46	0.42	0.45	0.34	0.39	0.46	0.64	0.65
Na_2O	0.02	0.01	0.01	0.02	0.02	0.01	0.02	0.02	0.02	0.02	0.01	0.02	0.02	0.02
K_2O	0.01	0.00	0.01	0.01	0.01	0.01	0.00	0.00	0.00	0.00	0.00	0.00	0.01	0.00
Mg#	0.87	0.87	0.70	0.71	0.65	0.64	0.49	0.49	0.68	0.68	0.60	0.60	0.53	0.53

Table 2 (continued)

Phase	Clinopyroxene average																	
Phase	Amphibole average																	
Sample	CB1042		CB1434		CB1424		CB1414		CB1475		CB1060		CB1482		SP0003			
Unit	UZ		UMZ		UMZ		UMZ		UMZ		UMZ		UMZ		SP			
Rock Type	websterite		gabbro		diorite		gabbro		gabbro		xenolith		Grt-diorite		amphibolite			
Strat Pos (m)	3514		4858		7053		7456		8221		9260		10557		12000			
Position	core	rim	core	rim	core	rim	core	rim	core	rim	core	rim	core	rim	core	rim		
SiO_2	44.96	45.05	43.84	46.06	43.59	42.83	48.32	48.63	45.67	44.87	43.46	43.48	43.88	44.49	44.53	44.82		
TiO_2	1.80	1.89	1.40	1.23	1.27	1.28	1.32	1.25	1.54	1.64	0.59	0.54	1.80	1.64	0.95	0.69		
Al_2O_3	13.66	13.38	13.30	13.09	12.20	13.53	9.75	9.58	10.83	12.07	16.74	16.77	11.63	11.91	11.28	11.89		
Cr_2O_3	1.62	1.91	0.17	0.11	0.05	0.02	0.65	0.59	0.09	0.14	0.03	0.04	0.03	0.03	0.06	0.07		
FeO_T	3.51	3.62	8.60	8.86	16.79	16.78	8.25	7.99	11.85	11.50	12.91	13.12	13.90	13.52	16.98	16.77		
MnO	0.05	0.05	0.11	0.08	0.17	0.19	0.11	0.09	0.10	0.10	0.08	0.07	0.05	0.04	0.26	0.26		
NiO	0.12	0.06	0.03	0.03	0.01	0.02	0.01	0.02	0.07	0.06	0.02	0.02	0.03	0.01	0.02	0.02		
MgO	16.59	16.66	14.02	14.32	9.76	9.38	15.45	15.73	13.01	12.72	10.33	10.33	11.39	11.45	9.57	9.54		
CaO	11.80	11.71	12.58	10.62	11.11	11.21	11.31	11.42	11.23	11.79	11.15	11.16	11.39	11.47	11.37	11.49		
Na_2O	2.19	2.17	1.64	1.61	1.49	1.56	1.23	1.14	1.23	1.24	1.51	1.50	1.50	1.48	1.41	1.29		
K_2O	0.64	0.65	1.00	0.90	0.58	0.68	0.53	0.52	0.92	1.01	0.32	0.32	1.17	1.12	0.37	0.35		
Mg#	0.89	0.89	0.74	0.74	0.51	0.50	0.77	0.78	0.66	0.66	0.59	0.58	0.59	0.60	0.50	0.50		
Phase	Plagioclase average																	
Sample	CB1042		CB1434		CB1464		CB1424		CB1414		CB1475		CB1060		CB1482		SP0003	
Unit	UZ		UMZ		UMZ		UMZ		UMZ		UMZ		UMZ		UMZ		SP	
Rock Type	websterite		gabbro		gabbro		diorite		gabbro		gabbro		xenolith		Grt-diorite		amphibolite	
Strat Pos (m)	3514		4858		4874		7053		7456		8221		9260		10557		12000	
Position	core	rim	core	rim	core	rim	core	rim	core	rim	core	rim	core	rim	core	rim	core	rim
SiO_2	48.09	47.89	49.83	49.38	48.64	48.09	45.90	45.65	47.83	47.42	48.69	48.45	47.55	47.06	47.75	49.06	47.90	46.66
TiO_2	0.02	0.00	0.02	0.02	0.01	0.02	0.00	0.03	0.01	0.02	0.02	0.01	0.00	0.01	0.01	0.02	0.01	0.02
Al_2O_3	33.50	34.00	33.50	33.75	33.30	33.54	35.20	35.36	34.14	34.32	33.08	33.22	33.88	34.22	33.79	32.84	33.87	34.57
Cr_2O_3	0.01	0.03	0.00	0.01	0.00	0.00	0.00	0.00	0.01	0.00	0.02	0.01	0.01	0.00	0.01	0.01	0.00	0.01
FeO_T	0.03	0.06	0.04	0.10	0.04	0.11	0.07	0.17	0.02	0.04	0.04	0.09	0.01	0.08	0.02	0.12	0.10	0.16
MnO	0.01	0.01	0.01	0.04	0.00	0.00	0.00	0.00	0.00	0.00	0.01	0.01	0.00	0.02	0.01	0.01	0.00	0.00
NiO	0.03	0.01	0.02	0.02	0.00	0.00	0.00	0.00	0.00	0.00	0.04	0.02	0.01	0.03	0.01	0.01	0.00	0.00
MgO	0.00	0.01	0.00	0.01	0.00	0.00	0.00	0.00	0.00	0.00	0.00	0.01	0.01	0.01	0.00	0.00	0.00	0.00
CaO	15.54	15.79	12.99	13.35	15.32	15.73	17.36	17.48	15.86	16.10	15.56	15.61	16.37	16.78	16.18	15.19	15.89	16.60
Na_2O	2.45	2.31	3.51	3.29	2.61	2.36	1.40	1.30	2.28	2.12	2.55	2.49	2.10	1.83	2.18	2.75	2.29	1.79
K_2O	0.03	0.03	0.07	0.06	0.07	0.06	0.02	0.01	0.03	0.02	0.06	0.05	0.02	0.02	0.04	0.03	0.01	0.01

Table 2 (continued)

Phase	Clinopyroxene average														
An	77.69	78.95	66.86	68.88	76.10	78.40	87.19	88.08	79.22	80.64	76.89	77.41	81.11	83.44	80.26	75.24	79.27	83.61
Ab	22.12	20.88	32.74	30.77	23.46	21.26	12.70	11.85	20.62	19.23	22.78	22.31	18.79	16.46	19.54	24.57	20.65	16.34
Or	0.19	0.16	0.41	0.36	0.44	0.34	0.11	0.07	0.16	0.13	0.33	0.28	0.10	0.10	0.21	0.19	0.08	0.05

Strat Pos (m) is the stratigraphic position in meters: i.e. the recalculated stratigraphic height from the base of the complex, taking into account the attitude of the layers

Mg# was calculated as $Mg^{2+}/(Mg^{2+}+Fe^{2+})$ molar ratio

An, Ab, and Or = anorthite, albite, and orthoclase molar fractions are reported for plagioclase analyses

For abbreviations of rock units (Unit) see the geological setting chapter

crystals show a reverse zoning, with rims enriched in anorthite (An) relative to cores (with the exception of sample CB1482; Tab. 2). Minerals from the garnet-amphibolite xenolith (sample CB1060) within the complex show no or poor zoning.

Amphibole and clinopyroxene, when co-existing, show similar REE patterns and equilibrium in the partition of trace elements (Fig. 12). When only clinopyroxene occurs, it shows higher trace element abundance compared to samples containing also amphibole (Fig. 12).

In the UZ pyroxenite sample CB1042, amphibole and clinopyroxene show similar patterns depleted in LREE (Fig. 12; $(La/Sm)_N$ = 0.41 and between 0.29–0.35 respectively; $(La/Yb)_N$ = 0.22 and between 0.15–0.19; values normalized to the Primitive Mantle, PM, Hofmann 1988). Both amphibole and clinopyroxene show a slightly negative Eu anomaly ($(Eu/Eu^*)_N$ = 0.86 and between 0.88–1.00), very low U, Th, Nb and Ta contents (<1) and similar Zr and Hf contents (Fig. 13; Zr = 12.06 ppm in amphibole and between 10.63–13.71 ppm in clinopyroxene; Hf = 0.59 ppm in amphibole and between 0.54–0.64 ppm in clinopyroxene).

Amphibole and clinopyroxene from UMZ gabbroic samples (samples CB1414, CB1464 and CB1475) have REE patterns depleted in LREE similar to the UZ sample (Fig. 12; $(La/Sm)_N$ = 0.58–0.62 in amphibole and between 0.25–0.61 in clinopyroxene; $(La/Yb)_N$ = 0.78–0.89 and 0.31–0.84, respectively). All the gabbroic samples cited above have a negative Eu anomaly (Fig. 12; $(Eu/Eu^*)_N$ = 0.35–0.47 for amphibole and 0.22–0.61 for clinopyroxene) related to plagioclase fractionation. Clinopyroxenes have similar $(Th/U)_N$, $(Zr/Hf)_N$ and $(Nb/Ta)_N$ ratios (Fig. 13; higher than 1 for $(Th/U)_N$ and lower for others respectively).

The two diorite samples (CB1424 and CB1482) show REE patterns enriched in LREE (Fig. 12; $(La/Sm)_N$ = 1.03–2.63 for amphibole and between 1.36–1.53 for clinopyroxene; $(La/Yb)_N$ = 1.28–186.58 and 1.56–1.65 respectively). Whereas amphiboles from sample CB1424 show t MREE-HREE trends almost flat and those from sample CB1482 show a strong depletion in MREE and HREE (Fig. 12). This may be an artefact of the co-existence of amphibole with garnet. Compared to gabbroic samples, clinopyroxenes from diorite CB1424 have a positive Eu anomaly ($(Eu/Eu^*)_N$ = 1.57–1.68 and 1.98–2.29 respectively). This feature was also observed in other layered complexes (e.g. the Val Sesia complex; Mazzucchelli et al. 1992) and was interpreted as the evidence of mixing between a mantle-derived melt and a crustal component derived from anatexis of granulite-facies metasediments. Amphibole and clinopyroxene from diorites have $(Th/U)_N$, $(Zr/Hf)_N$ and $(Nb/Ta)_N$ ratios similar to gabbros (Fig. 13).

Amphibole from the garnet-amphibolite xenolith (classified as Tschermakite, sample CB1060) is depleted in HREE,

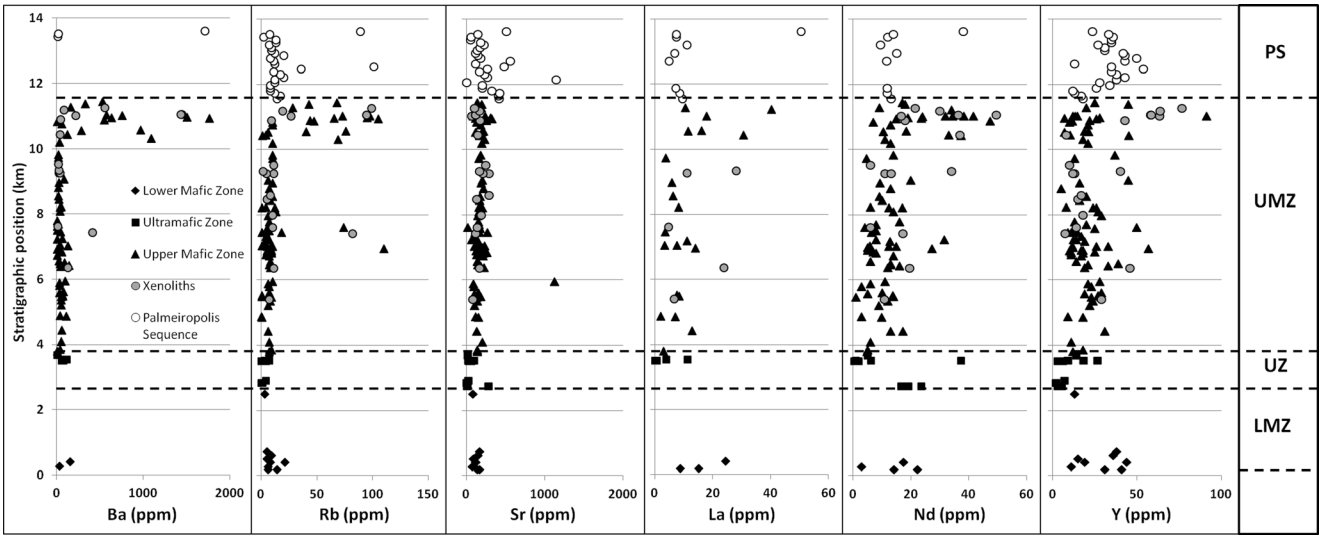

Fig. 5 Plot of bulk-rock trace element concentrations (in ppm) along the stratigraphy of the Cana Brava complex

suggesting equilibrium with Garnet (Fig. 12; $(Sm/Yb)_N$ = 5.61–19.48), and in LREE, suggesting depletion during the incorporation within the complex (Fig. 12; $(La/Sm)_N$ = 0.08–0.13). Conversely, amphibole (classified as Hornblende) and clinopyroxene from the amphibolite of the Palmeirópolis Sequence show almost flat REE patterns, with a slight enrichment in LREE of clinopyroxene compared to amphibole (Fig. 12; $(La/Sm)_N$ = 0.74–0.98 and 1.32–1.94 respectively; $(La/Yb)_N$ = 0.58–0.87 and 0.89–1.37). Amphibole from garnet-bearing amphibolite (sample CB1060) has negative $(Th/U)_N$, $(Zr/Hf)_N$ and $(Nb/Ta)_N$ ratios (Fig. 13), while amphibole from Palmeirópolis Sequence sample (SP0003) has positive $(Zr/Hf)_N$ and $(Nb/Ta)_N$ ratios (Fig. 13). Differently from the amphibole, clinopyroxene from sample SP0003 has negative $(Zr/Hf)_N$ ratio (Fig. 13).

Discussion

Metamorphic overprint versus syn-magmatic deformation

The widespread high-T foliation and common hypersolidus deformation structures (see the *field evidences* chapter) indicate

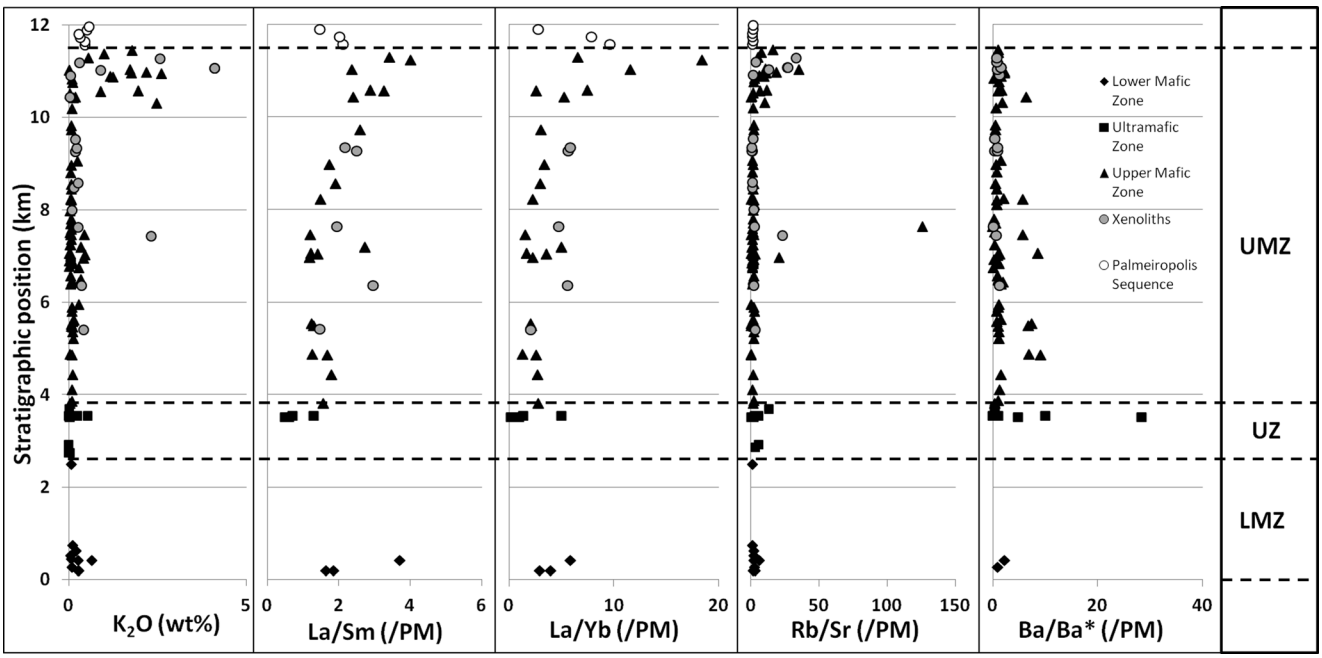

Fig. 6 Plot of bulk-rock K_2O and trace elements ratios normalized to the Primitive Mantle (PM; Hofmann 1988) along the stratigraphy of the Cana Brava complex

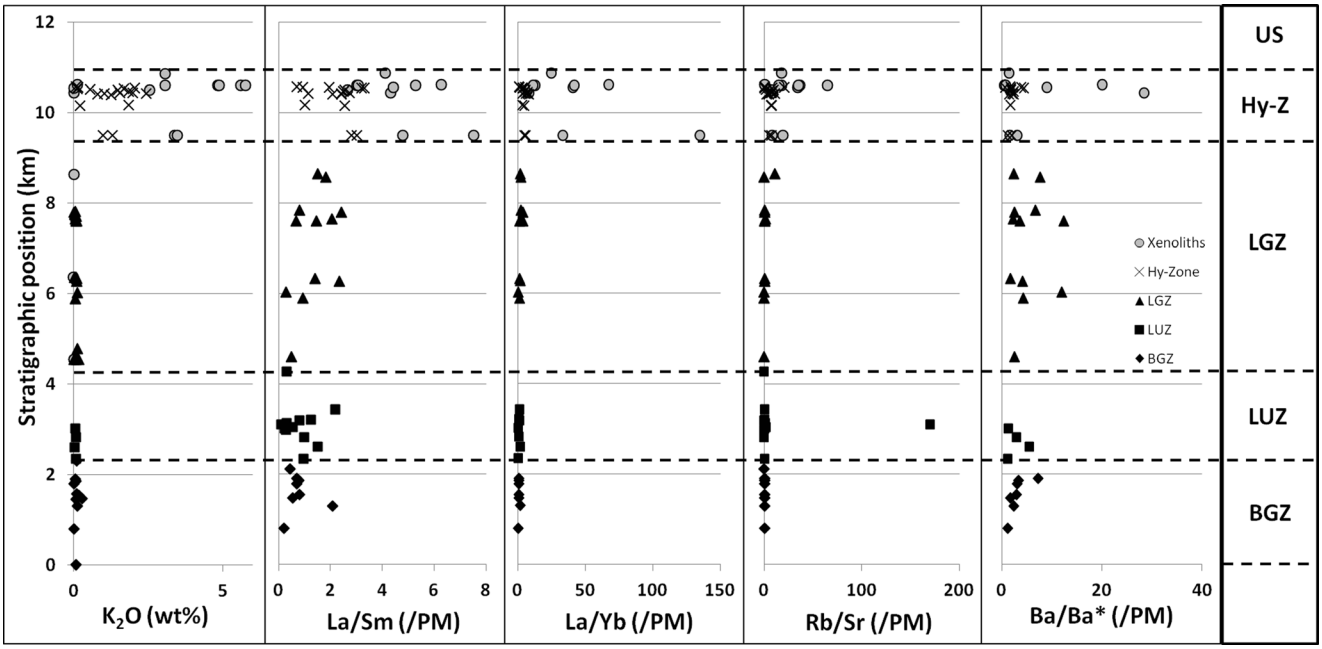

Fig. 7 Plot of bulk-rock K_2O and trace elements ratios normalized to the Primitive Mantle (PM; Hofmann 1988) along the stratigraphy of the Niquelândia complex

that the Cana Brava complex underwent hyper-to-sub solidus deformation during its intrusion, in the same way of the Niquelândia complex (Correia et al. 2012). The close similarity of the metamorphic age (770–760 Ma of Ferreira Filho et al. 2010) and the crystallization ages (800–770 Ma of Ferreira Filho et al. 2010 and Giovanardi et al. 2015) reported in the literature, reinforce the interpretation that the granulite facies foliation and re-crystallization are not related to a later metamorphic event but a consequence of stretching during the intrusion growth. The 770–760 Ma recrystallization age of Niquelândia, inferred as metamorphic by Pimentel et al. (2004a), was later reinterpreted by Ferreira Filho et al. (2010) as indicative of the regional metamorphism that affected also Cana Brava and Barro Alto. This age is based on a concordant U-Pb SHRIMP analysis on low Th/U zircon rims from sample CF-04 (765 ± 8 Ma) (Pimentel et al. 2004a) and on a Sm-Nd garnet age of a metasediment sample (MR-137 A) from the Mara Rosa Arc at 760 ± 75 Ma (Junges et al. 2002). As pointed out by Correia et al. (2012), sample CF-04 is likely a xenolith incorporated within Niquelândia (Pimentel et al. 2004a describe the sample as a 'quartz-rich mylonitic rock from a shear zone cutting through gabbros of the Upper Complex' and containing garnet and quartz with accessory plagioclase, kyanite ilmenite and zircon). Sample MR-137 A, instead, belongs to a unit outcropping more than 100 km away from the Niquelândia complex and seems unrelated to the complexes intrusion. We infer that the rims of several zircons from sample CF-04 record the incorporation of the xenoliths in the mafic magma rather than a separate metamorphic overprint. Moreover, the Sm-Nd garnet age from the metasediment of the Mara Rosa Arc, if related to the studied area, records an age indistinguishable, within error, from the crystallization age of the complexes. Therefore, we conclude that, like in Niquelândia, the Cana Brava complex did not experience a later metamorphic event (Correia et al. 1997) or granulite-facies metamorphism (Ferreira Filho et al. 2010; Biondi 2014), and that the high-T "metamorphic" features are a consequence of shear of a crystallizing crystal mush during the growth of the complex. This hypothesis is also supported by mineral geochemistry. Minerals from the complex show igneous zoning (Table 2). The reverse zoning of plagioclase is common in several magmatic contexts and is generally interpreted as the evidence of i) diminishing P conditions, ii) mixing with a new input of mafic melt or iii) increase of the H_2O in the residual melt (Sisson and Grove 1993; Singer et al. 1995 and references therein). The increase of CaO content in all phases along the stratigraphy (Table 2) rules out that the reverse zoning is an effect of subsolidus re-crystallization because it should have depleted the other phases in Ca. However, the present data does not allow discriminating the process responsible for the inverse plagioclase zonation. Mg# correlation between the main mafic phases (i.e. clinopyroxene, orthopyroxene and amphibole) shows excellent linear trends (Fig. 11; R^2 = 0.95–0.98). Trace elements distribution between coexisting amphibole and clinopyroxene shows equilibrium patterns (e.g. samples CB1042, CB1414 and CB1424, Fig. 13). Magmatic zonations and the trace elements equilibrium between amphibole and clinopyroxene are consistent with crystallization of these phases from the same melt and not with metamorphic recrystallization. Amphibole absence results in higher trace elements abundance in

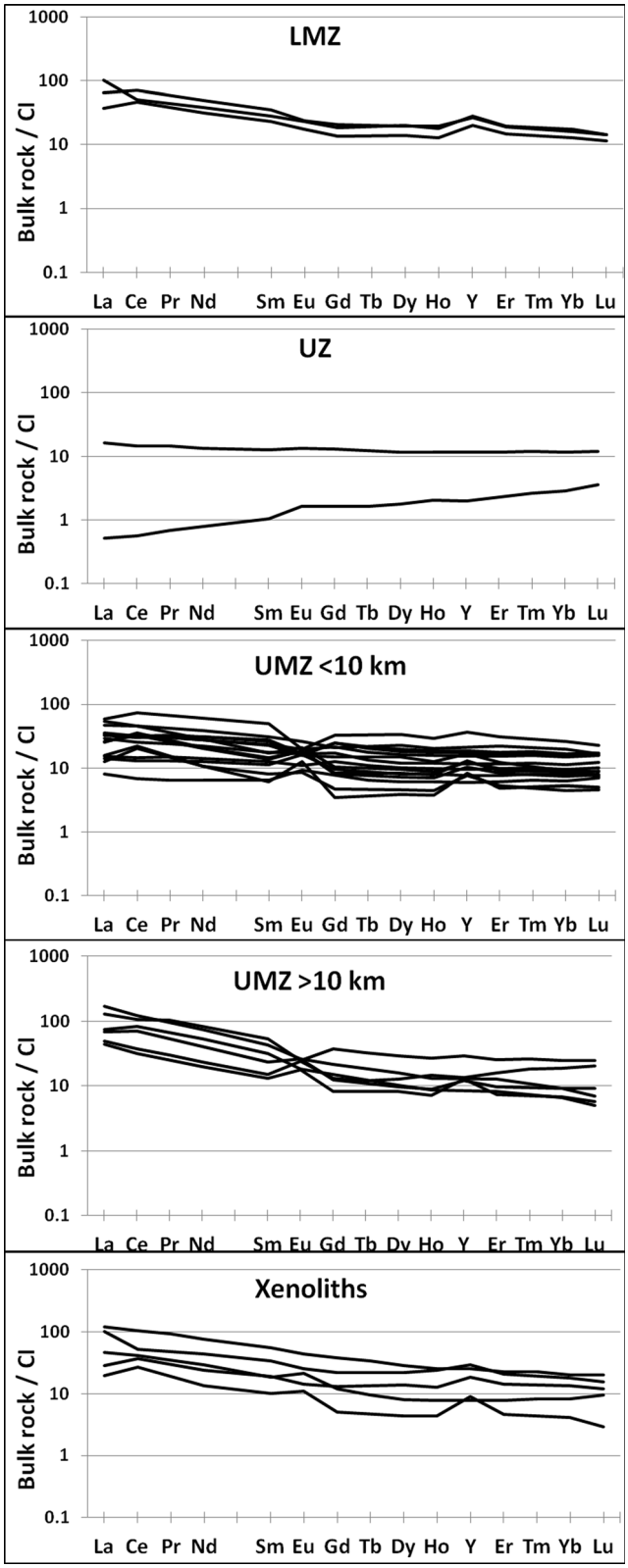

Fig. 8 Plot of bulk-rock REE patterns normalized to the Chondrite I composition (CI; Anders and Edibara 1992)

clinopyroxene (Fig. 13), possibly because this is the only phase that can incorporate them.

In contrast, phase composition and textural evidences of the amphibolite sample from the Palmeirópolis Sequences (SP0003) suggest that amphibole and clinopyroxene are not in equilibrium in this rock. In particular, clinopyroxene occurs as relict often partially substituted by amphibole in small-grain bands. The trace element distribution show that clinopyroxene is slightly enriched in LREE ($(La/Sm)_N$ 1.32–1.94) whereas amphibole is slightly depleted ($(La/Sm)_N$ 0.74–0.98; Fig. 12). Clinopyroxene major element composition is similar to that one reported by Ferreira Filho et al. (1999) for the metamorphic clinopyroxene of the Juscelândia Sequence metabasalt (i.e SiO_2 > 52 wt%, Al_2O_3 < 2 wt% and CaO > 22 wt%; Table 2), whereas the plagioclase composition is similar to the igneous plagioclase in the metabasalt (i.e. An =78.5–85.0 %, Ferreira Filho et al. 1999; Table 2). These observations suggest that sample SP0003 is only partially recrystallized by the metamorphic event that affected the metavolcanic-metasedimentary sequences (Ferreira Filho et al. 2010 and references therein). Conversely, amphibole from the garnet-amphibolite within the complex (CB1060) does not show crystal zonation and the plagioclase zonation is minor compared to the Palmeirópolis amphibolite (Fig. 13). The amphibole has trace elements patterns in equilibrium with the garnet (Figs. 12 and 13). The absence of phase zonation and the amphibole/garnet trace elements equilibrium and LREE depletion suggest that sample CB1060 was more re-equilibrated than the amphibolite of Palmeirópolis (sample SP0003). The more evolved re-equilibration of the xenoliths in comparison to the partial re-equilibration of the Palmeirópolis amphibolite, is consistent with the protracted entrapment (or sinking) of the xenolith within a substantial amount of magma.

Geothermometry

We used four different geothermometers to evaluate the temperature of the Cana Brava parent melt and the temperature reached by the xenoliths. Data are reported in °C in Table 3. For gabbroic rocks of the complex, we used the Fe-Mg exchange between clinopyroxene and orthopyroxene (Wells 1977), the Ca and Al in orthopyroxene and clinopyroxene (Mercier 1980) and the amphibole-plagioclase equilibrium (Holland and Blundy 1994). Two xenolith samples were investigated: the garnet-amphibolite CB1060, using the Holland and Blundy (1994) geothermometer, and the quartzite CB1425. Quartz crystals from the latter were studied in cathodoluminescence (Fig. 14) and analysed for Ti by LA-ICP-MS to estimate the "Ti in quartz temperature" according to Thomas et al. (2010). The temperature of an amphibolite of the Palmeirópolis Sequence was estimated using the Holland and Blundy (1994) geothermometer.

Temperatures of the gabbroic rocks obtained with the geothermometers of Wells (1977) and Mercier (1980) range between 819 and 993 °C and 879–1144 °C,

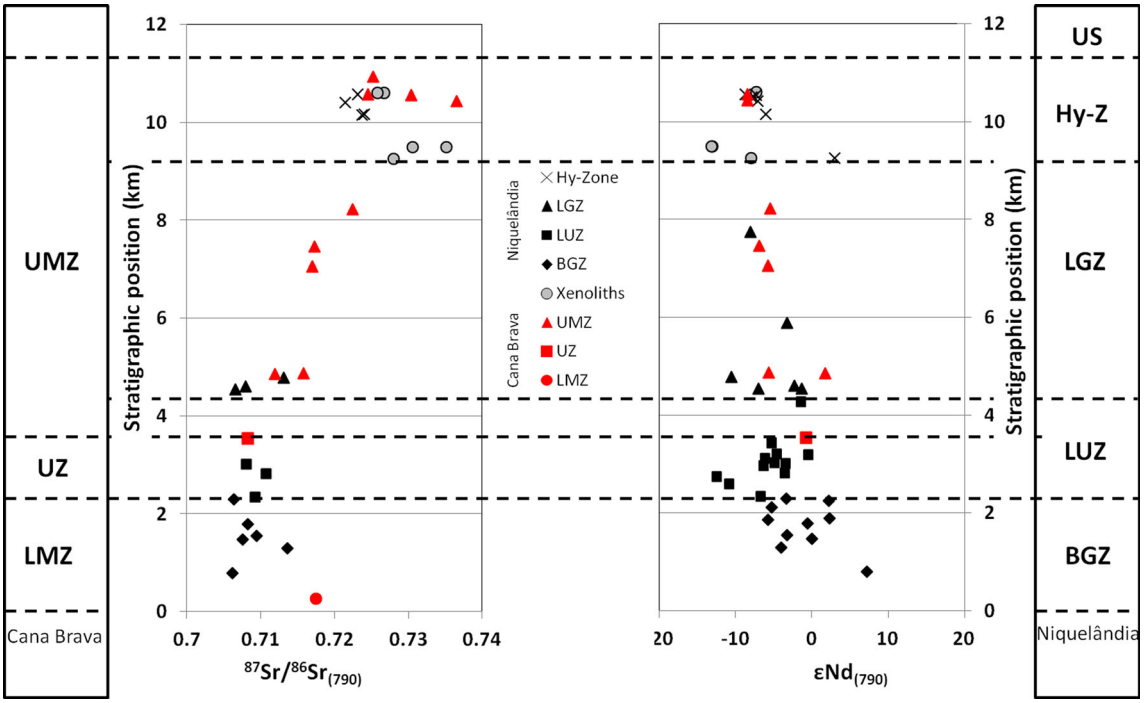

Fig. 9 Plot of $^{87}Sr/^{86}Sr$ ratio and εNd recalculated to 790 Ma of samples from the Niquelândia (Correia et al. 2012) and Cana Brava complexes along the stratigraphy

respectively, and differ by about 150 °C. Temperatures obtained with the Holland and Blundy (1994) geothermometer show intermediate values in the range of 879–995 °C, but closer to those calculated according to Wells (1977) (Table 3; Fig. 15). Notwithstanding the differences, all temperatures are high and we interpret them as closure temperatures of the different systems during the crystallization of the complex.

The temperatures estimated for the garnet-amphibolite xenolith according to the thermometer of Holland and Blundy (1994) range from 866° to 956 °C and are comparable to those obtained for the gabbroic rocks (Table 3; Fig. 15). This suggests that the xenolith attained granulite-facies conditions after its incorporation into the complex.

We used the Ti in quartz geothermometer of Thomas et al. (2010) to estimate temperatures along two cm-large crystal

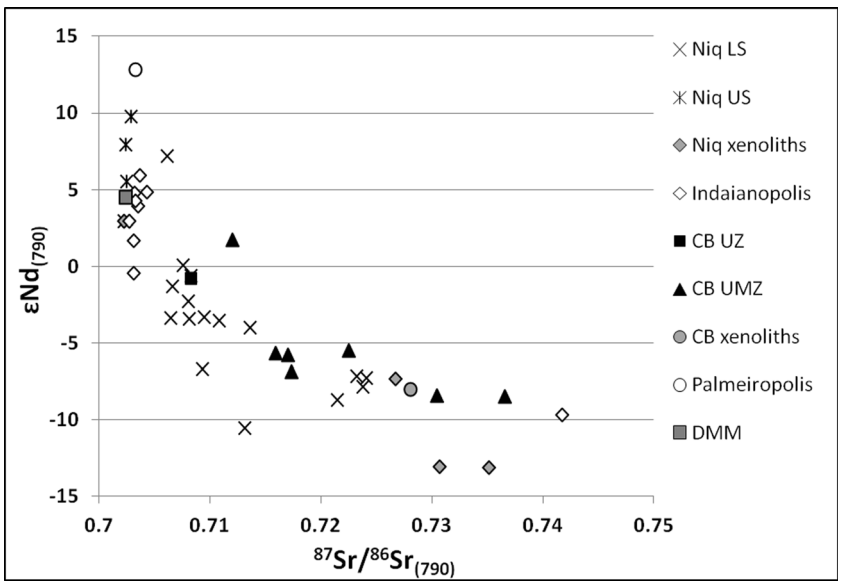

Fig. 10 Plot of εNd and $^{87}Sr/^{86}Sr$ ratio recalculated to 790 Ma of samples from the Niquelândia (Correia et al. 2012) and Cana Brava complexes. DMM is the Depleted Mantle MORB from Workman and Hart (2005)

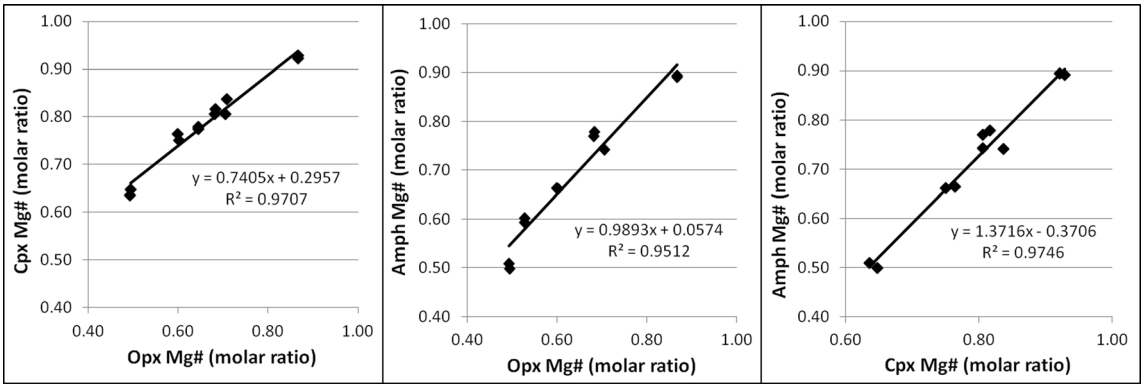

Fig. 11 Plot of Mg/(Mg + Fe) (Mg#, as molar ratio) of coexisting minerals in UZ and UMZ Cana Brava rocks

transects (Fig. 14). Due to the absence of other Ti-rich phases, the α TiO_2 was fixed at 0.1 and the pressure at 6 kbar (the minimum pressure estimated in literature for the crystallization of the complex). Temperatures estimated for the one crystal are

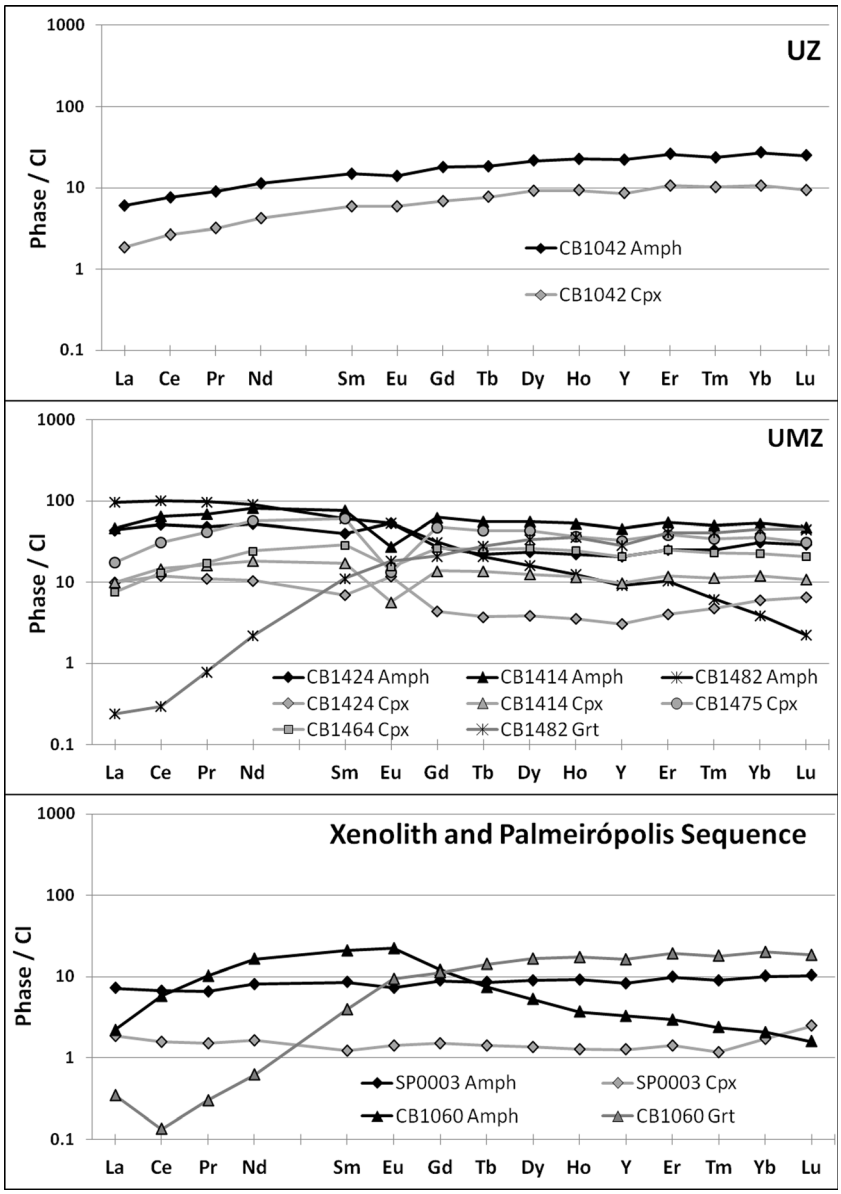

Fig. 12 Plot of amphibole, clinopyroxene and garnet REE (and Y) compositions of analysed samples from the different units, normalized to the Chondrite I (CI; values from Anders and Edibara 1992)

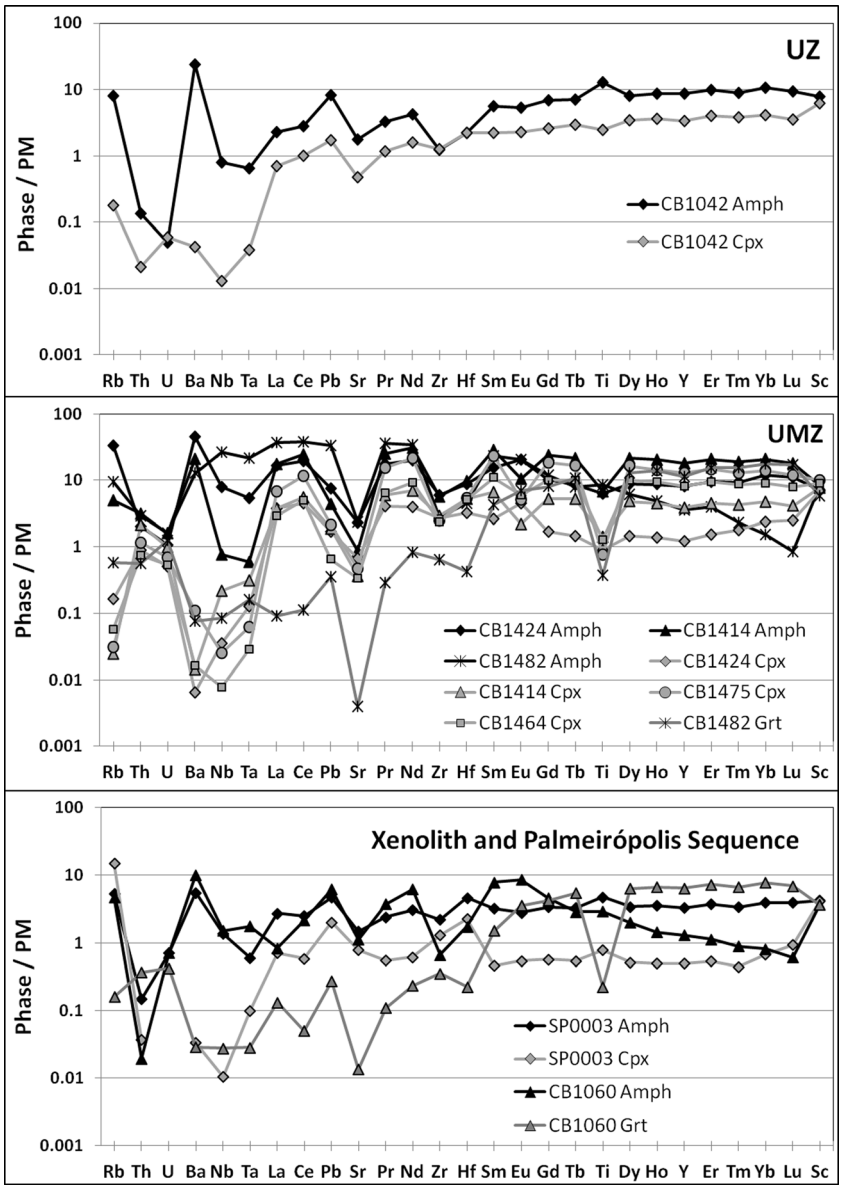

Fig. 13 Plot of amphibole, clinopyroxene and garnet trace element compositions of analysed samples from the different units, normalized to the Primitive Mantle (PM; values from Hofmann 1988)

much lower than the other, ranging between 669 and 886 °C and 735°-1157 °C, respectively (Table 3; Fig. 15). Possibly, the highest values represent the heating of the quartzite layer during its permanence in the magma batch, consistent with its location in the complex at a level deeper than the garnet-amphibolite. The high T reached by the xenoliths is consistent with their restitic composition after melt extraction.

Contamination process and comparison with the Niquelândia complex

Based on Sr isotopic ratios, Correia et al. (1997) proposed that the Cana Brava complex was affected by crustal contamination. The new isotopic data and the revision of the geochemical data support this hypothesis as explained here below (Figs. 9 and 10).

The K_2O, LILEs, Rb and Ba content in the rocks of the Cana Brava complex show constant values or a mild enrichment along stratigraphy, followed by higher values and a large spread approaching the roof (from 10 km; Figs. 5 and 6). The UZ pyroxenites show LREE depletion and flat trends (Fig. 8) consistent with cumulates from a MORB magma similar to the one estimated as the Cana Brava parental melt by Correia and Girardi (1998). The LREEs in the UMZ whole rock show a continuous increase upwards ($(La/Sm)_N$ range from 1.18 to 4.01; Figs. 6 and 8). Similarly to the $(La/Sm)_N$, the Rb-Sr and Sm-Nd isotopes along the Cana Brava stratigraphy show a gradual increase of contamination approaching the roof (Fig. 9). These features suggest that the contamination affected the entire magma column during the UMZ crystallization and was more intense in the igneous rocks containing abundant xenoliths, particularly in the

Table 3 Minimum, maximum, average and median temperature values (in °C) for selected samples, calculated based on the Fe-Mg exchange between clinopyroxene and orthopyroxene (Wells 1977), the Ca and Al in orthopyroxene and clinopyroxene (Mercier 1980), the amphibole-plagioclase equilibrium (Holland and Blundy 1994) and the Ti-in quartz (Thomas et al. 2010)

			Wells (1977)				Mercier (1980)				Holland and Blundy (1994)				Thomas et al. (2010)			
Sample	Unit	Strat Pos (m)	min	max	mean	median	min	max	mean	median	min	max	mean	median	min	max	mean	median
CB1042	UZ	3514	780	905	851	853	733	972	879	896	973	1012	995	998				
CB1434	UMZ	4858	926	1094	993	996	1096	1248	1144	1133	870	889	879	880				
CB1425	Xen	4865													669	1157	801	715
CB1464	UMZ	4874	792	858	819	815	985	1046	1005	999								
CB1424	UMZ	7053	823	888	848	844	1045	1117	1071	1071	791	989	898	906				
CB1414	UMZ	7456	859	962	905	899	1031	1131	1072	1069	945	1008	977	972				
CB1060	Xen	9260									866	956	926	930				
CB1475	UMZ	8221	808	950	852	834	1014	1149	1065	1048	870	903	886	886				
CB1482	UMZ	10,557									763	1017	942	953				
SP0003	SP	13,530									766	919	859	873				

Strat Pos (m) is the stratigraphic position in meters: i.e. the recalculated stratigraphic height from the base of the complex, taking into account the attitude of the layers

For abbreviations of rock units (Unit) see the geological setting chapter

uppermost 2 km of the complex. Locally, an increase of the contamination due to xenoliths contribution is supported by the spread of $^{87}Sr/^{86}Sr_{(790)}$ ratios observed at the roof of the complex ($^{87}Sr/^{86}Sr_{(790)}$ = 0.724609–0.736590), where xenoliths are more abundant, and by isotopes of the two samples at the base of the UMZ (CB1434 and CB1464, $^{87}Sr/^{86}Sr_{(790)}$ = 0.711978, 0.715871 and $\varepsilon Nd_{(790)}$ = 1.70, −5.65 respectively; Table 1; Figs. 9 and 10), which are close to a quartzite layer (sample CB1425).

These geochemical features are extremely similar to what has been observed in the Lower Sequence of the Niquelândia complex by Rivalenti et al. (2008) and Correia et al. (2012). They demonstrated that the lower units of the Niquelândia complex reached maximum contamination in the Hydrous Zone (Fig. 9; Correia et al. 2012). Conversely, the upper unit of Niquelândia (i.e. the Upper Gabbro-Anorthosite Zone, UGAZ of Girardi et al. 1986) is poorly or not contaminated (Fig. 10). In the Hydrous Zone, the contamination is shown by an anomalous increase of the most incompatible elements (e.g. K_2O, LREE, Rb and Ba) and by the Rb-Sr and Sm-Nd isotope ratios (Rivalenti et al. 2008). Based on the random variation of the contamination degree along the stratigraphy of the Niquelândia complex (Fig. 9), Rivalenti et al. (2008) and Correia et al. (2012) proposed that crustal contamination began later and locally, during the growth of the complex, when the parental melt had already fractionated the ultramafic units (i.e. the Basal Gabbro Zone, BGZ, the Basal Peridotite Zone, BPZ and the Layered Ultramafic Zone, LUZ; Girardi et al. 1986). According to them, the anorthositic crystal mush, which crystallized the upper Niquelândia sequence, was segregated during this first stage, and the buoyant crystal mush escaped the contamination that later affected the mafic magma in the proximity of the incorporated crustal levels (Rivalenti et al. 2008; Correia et al. 2012).

Apart from the absence of anorthosites, the Cana Brava complex shares many characteristics with the Lower Sequence of

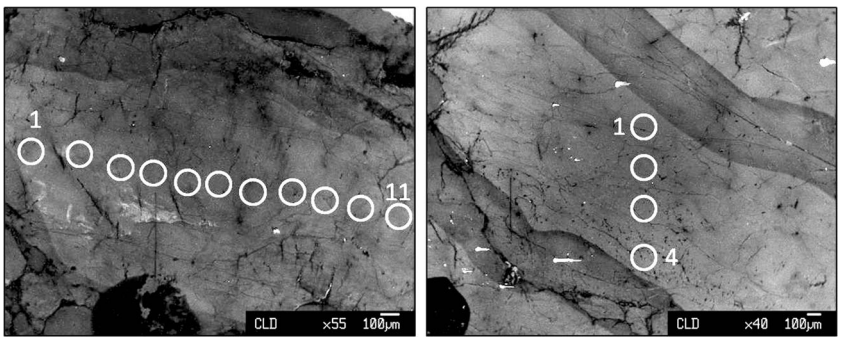

Fig. 14 Selected CL images of quartz grains in sample CB1425. Circles are LA-ICP-MS analysis points

Niquelândia. The parental melts estimated for the two complexes by Correia et al. (2012) and Correia and Girardi (1998) are very similar and inferred to be picritic MORB in composition. Thus, we propose that the contamination in Cana Brava has occurred as in Niquelândia, beginning after the fractionation of the ultramafic units, as proposed by Rivalenti et al. (2008) and Correia et al. (2012), and coupling an in situ effect driven by the abundance and composition of crustal xenoliths with a process at the scale of the whole complex (an AFC as proposed by Rivalenti et al. 2008).

Evidences for a single large intrusion

Ferreira Filho (1998) were the first one to propose, based on the similarity of ages and stratigraphy, that the three large layered intrusions constitute an originally continuous magmatic structure. Carminatti (2006) suggested a similar hypothesis based on gravimetric and geophysical evidences. However, Ferreira Filho et al. (2010) inferred that the three complexes might be distinct intrusions, because of the slightly younger age of the Cana Brava complex compared to the ages of Barro Alto and Niquelândia (Cana Brava c.a. 780 Ma, Niquelândia and Barro Alto c.a. 800–790 Ma).

More recently, SHRIMP ages obtained by Giovanardi et al. (2015) for Cana Brava yielded an ~800–780 Ma age, slightly older than the age obtained by Ferreira Filho et al. (2010) and close to the age of Niquelândia by Correia et al. (2012). Therefore, we conclude that the three complexes have, within errors, the same age and possibly could be part of a single body.

Fig. 16 Comparison of the Niquelândia and Cana Brava complexes. The Niquelândia map is modified from Correia et al. (2012) and the Cana Brava map is from this work

Not taking into account the Barro Alto complex, we will compare now the Niquelândia and Cana Brava complexes. Both Cana Brava and Niquelândia grew in a syn-magmatic stress field that caused hypersolidus foliation and re-crystallization of the igneous textures. Attitudes of banding and foliation in both complexes are similar (10–20° NNE, 30–50°W dip). Considering the two bodies as fragments of a single mafic batolith, it is possible to notice a progressive, northwards attenuation of the banding. In particular, the thickness of the cumulus peridotite decreases from ~2 km in the southern side of Niquelândia to ~1 km in the southern Cana Brava body and vanishes towards the North (Fig. 16). Moreover, the pyroxenite band, which is about 1 km thick in southern Niquelândia, diminishes to about 500 m in southern Cana Brava, turns northwards into a swarm of thin pyroxenite bands interlayered with gabbro and disappears in the northern sector (Fig. 1). In addition, in Niquelândia the upper anorthositic sequence of the complex is thick in the south and reduced northwards, and does not exist in Cana Brava (Fig. 16).

We re-calculated the estimated thickness of Cana Brava in the southern part of the complex to about 12 km (Figs. 1 and 16) and this value matches the thickness of the Niquelândia Lower Sequence at its northern end (Correia et al. 2012). The stratigraphic, structural, geochronological and geochemical

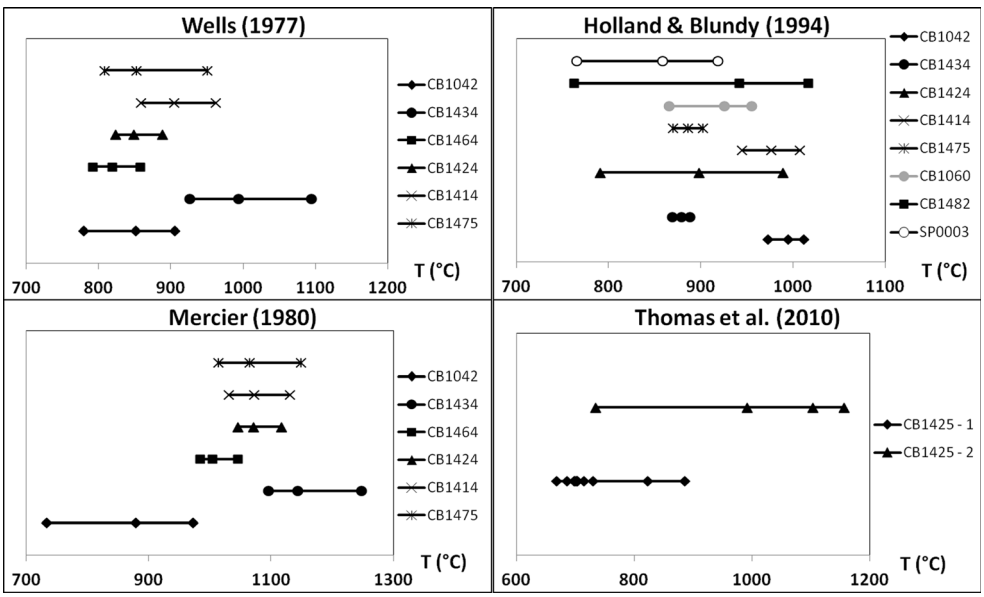

Fig. 15 Plot of temperatures (maximum, average and minimum) calculated using the geothermometers of Wells (1977), Mercier (1980) and Holland and Blundy (1994). Temperatures from all analyses on quartzite based on the Ti in quartz geothermometer (Thomas et al. 2010) calculated at 6 kbar and assuming α $TiO_2 = 0.1$ due to the absence of other phases except for quartz

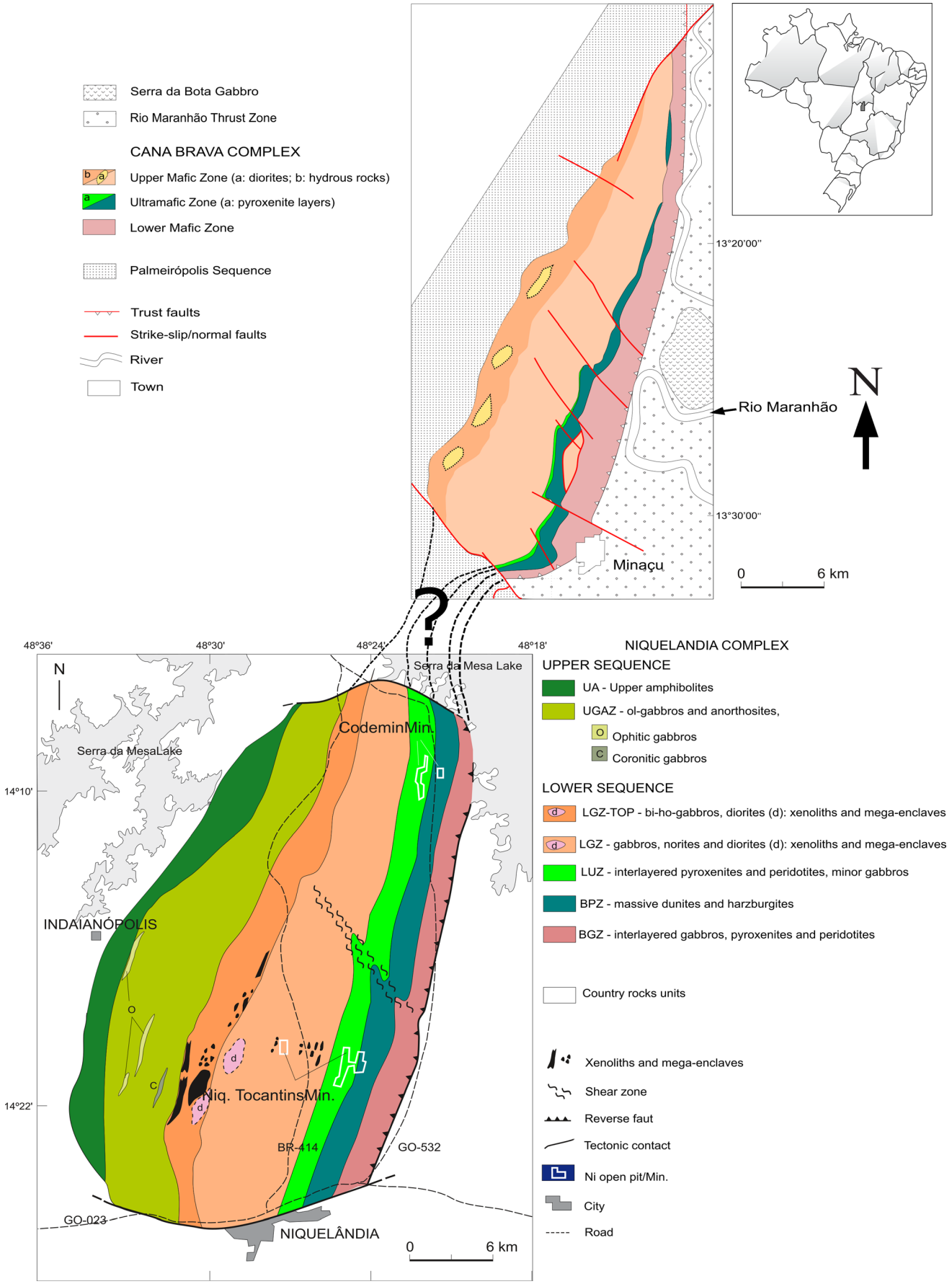
Serra da Bota Gabbro
Rio Maranhão Thrust Zone
CANA BRAVA COMPLEX
Upper Mafic Zone (a: diorites; b: hydrous rocks)
Ultramafic Zone (a: pyroxenite layers)
Lower Mafic Zone
Palmeirópolis Sequence
Trust faults
Strike-slip/normal faults
River
Town
13°20'00"
13°30'00"
Rio Maranhão
Minaçu
N
0
6 km
48°36'
48°30'
48°24'
48°18'
14°10'
14°22'
Serra da Mesa Lake
Serra da MesaLake
CodeminMin.
INDAIANÓPOLIS
Niq. TocantinsMin.
BR-414
GO-532
GO-023
NIQUELÂNDIA
NIQUELANDIA COMPLEX
UPPER SEQUENCE
UA - Upper amphibolites
UGAZ - ol-gabbros and anorthosites,
Ophitic gabbros
Coronitic gabbros
LOWER SEQUENCE
LGZ-TOP - bi-ho-gabbros, diorites (d): xenoliths and mega-enclaves
LGZ - gabbros, norites and diorites (d): xenoliths and mega-enclaves
LUZ - interlayered pyroxenites and peridotites, minor gabbros
BPZ - massive dunites and harzburgites
BGZ - interlayered gabbros, pyroxenites and peridotites
Country rocks units
Xenoliths and mega-enclaves
Shear zone
Reverse faut
Tectonic contact
Ni open pit/Min.
City
Road

similarities between the two sequences support the hypothesis that the Cana Brava and Niquelândia complexes are part of a single large intrusion. In Cana Brava, hydrous phases increase in gabbroic and dioritic rocks approaching the roof, same as in the Hydrous Zone of Niquelândia. In both cases, the increase in hydrous phases is associated to the common presence of crustal xenoliths. Similarly, both complexes show an increase in contamination along the stratigraphy and up to the roof. The isotopic and geochemical variations are comparable (Figs. 6, 7, 9 and 10).

At the southern end of Cana Brava, the convergence of banding and foliation suggests a sort of mega-boudinage of the entire complex (Figs. 1 and 16) (Correia et al. 1997; Correia and Girardi 1998; Ferreira Filho et al. 2010), possibly caused by tectonics during the exhumation of the complexes. According to Rivalenti et al. (2008) and Correia et al. (2012), the Upper Sequence of the Niquelândia complex consists mainly of anorthosites formed by segregation of the anorthositic crystal mush after fractionation of abundant peridotite cumulates. In Cana Brava, their absence is associated to a reduced thickness of the cumulus peridotite. Possibly, the anorthositic crystal mush formed only above the most important feeding centre(s), located somewhere in correspondence of Niquelândia. The decrease in thickness of the Upper Sequence of the Niquelândia complex to the North suggests that the anorthosite bands tend to disappear in this direction. However, the lack of outcrops between Cana Brava and Niquelândia hides this feature in the field. Therefore, based on all new and old geochemical data and field observations we conclude that Cana Brava and Niquelândia are fragments of a single body.

Conclusions

Field and geochemical evidences are consistent with an incremental growth of the Cana Brava body in a stress field that produced a sin-magmatic to high-T foliation and a granoblastic recrystallization. Structural, geochronological and mineralogical data indicate that the foliation and re-crystallization were not related to a later metamorphic event as formerly proposed, but were the consequence of stretching during the emplacement of the complex. The new chemical and isotopic data presented in this paper demonstrate that the Cana Brava complex was contaminated during its growth, similarly to what has been observed in the Lower Sequence of Niquelândia. The contamination in the Cana Brava complex shows an effect at the local scale as revealed by the spread of trace elements and isotope values near xenoliths-rich layers and a general enrichment along the stratigraphy, suggesting a progression of the contamination during the growth of the complex.

The Cana Brava complex and the Lower Sequence of Niquelandia share very similar chemical and textural characteristics and have, within error, the same age. Considered collectively, the two complexes show a continuous northwards thinning of the entire body as well as of individual bands (e.g. the ultramafic level). All these observations lead us to conclude that, most likely, the two complexes are separate parts of a single, large mafic body.

Acknowledgments Constructive comments by an anonymous reviewer, Cesar F. Ferreira Filho, Fernando Gervilla and Lutz Nasdala helped us improve the manuscript and are gratefully acknowledged. Anna Cipriani is deeply thanked for the stimulating discussion that improved the manuscript. Tommaso Giovanardi acknowledges the financial support of the Research Support Foundation of the State of São Paulo (FAPESP) in the frame of project 2013/19519-6. We would also like to thank the following institutions for the permission to use analytical facilities: the Mineralogy and Geotectonic Departament of the Universidade de São Paulo (Brazil) for the bulk rock major and trace element analyses, the Geochronological Research Centre of the Universidade de São Paulo (Brazil, IGc-CPGeo-USP) for the Sm-Nd and Rb-Sr isotopic analyses, the University of Milano (Italy) for the electron microprobe and cathodoluminescence analyses, the Centro Interdipartimentale Grandi Strumenti (C.I.G.S.) of the University of Modena and Reggio Emilia for the LA-ICP-MS.

References

Anders E, Edibara M (1992) Solar system abundances of the elements. Geochim Cosmochim Ac 46:2363–2380

Araújo,SM (1996) Geochemical and isotopic characteristics of alteration zones in highly metamorphosed volcanogenic massive sulfide deposits and their potential application to mineral exploration. Unpublished Ph.D. Thesis, Department of Geology, University of Toronto, Canada, pp 1–210

Araújo SM, Fawcett JJ, Scott SD (1995) Metamorphism of hydrothermally altered rocks in a volcanogenic massive sulfide deposit: the Palmeirópolis, brazil, example. Rev Bras Geosci 25(3):173–184

Biondi JC (2014) Neoproterozoic Cana Brava chrysotile deposit (Goiás, Brazil): geology and geochemistry of chrysotile vein formation. Lithos:184–187

Brod JA, Jost H (1991) Características estruturais, litológicas e magmáticas da zona de cisalhamento dúctil do Rio Traíras, bloco do Complexo Niquelândia, Goiás. Rev Bras Geosci 21:205–217

Carminatti MG (2006) Modelagem geofisica dos corpos maficos-ultramaficos de Cana Brava, Niquelandia e Barro Alto, centro de Goias. PhD Thesis for the Universidade de São Paulo (Brazili), Instituto de Geociências, pp 1–293

Correia CT, Girardi VAV (1998) Geoquimica e petrologia das rochas maficas e ultramaficas do complexo estratiforme de Cana Brava - GO, e das suas encaixantes. Bol Inst Geociências USP 29:1–37

Correia CT, Girardi VAV, Tassinari CG, Jost H (1997) Rb-Sr and Sm-Nd geochronology of the Cana Brava layered mafic-ultramafic intrusion, Brasil, and considerations regarding its tectonic evolution. Rev Bras Geosci 27(2):163–168

Correia CT, Jost H, Tassinari CCG, Girardi VAV, Kinny PD (1999) Ectasian Mesoproterozoic U–Pb ages (SHRIMP II) for themetavolcano-sedimentary sequences of Juscelandia and Indaianopolis and for the high grade metamorphosed rocks of the Barro Alto stratiform igneous complex, Goiàs State, Central Brasil. II° South Am Symp Isotopic Geology, Cordoba, Argentina, Actas, pp 31–33

Correia CT, Girardi VAV, Basei MAS, Nutman A (2007) Cryogenian U–Pb (Shrimp I) zircon ages of anorthosites from the upper sequences of Niquelandia and Barro Alto Complexes, Central Brasil. Rev Bras Geosci 37:70–75

Correia CT, Sinigoi S, Girardi VAV, Mazzucchelli M, Tassinari CCG, Giovanardi T (2012) The growth of large mafic intrusions: comparing Niquelandia and Ivrea igneous complexes. Lithos 155:67–182

Della Giustina MES, Pimentel MM, Ferreira Filho CF, Fuck RA, Andrade S (2011) U–Pb–Hf-trace element systematics and geochronology of zircon from a granulite-facies metamorphosed mafic–ultramafic layered complex in Central Brazil. Precambrian Res 189: 172–192

Dreher AM, Girardi VAV, Comin-Chiaramonti P (1989) Petrología dos rodingitos do complexo máfico-ultramáfico de Cana Brava, Goiás. Rev Bras Geosci 19(2):224–236

Feininger T, Dantas JJ, Girardi VAV (1991) Gravity interpretation and possible regional significance of the Niquelândia layered basic–ultrabasic complex, Goiàs, Brasil. J S Am Earth Sci 4:343–350

Ferreira Filho CF (1998) Geology and petrology of the large layered intrusions of central Brazil: implications for PGE mineralization. In: Platinum Symposium, Rustemburg, South Africa, Extended Abstracts, pp 107–110

Ferreira Filho CF, Pimentel MM (2000) Sm–Nd isotope systematics and REE–Hf–Ta–Th data of troctolites and their amphibolitized equivalents of the Niquelândia complex upper layered series, Central Brazil: further constraints for the timing of magmatism and high-grade metamorphism. J S Am Earth Sci 13:647–659

Ferreira Filho CF, Nilson AA, Naldrett AJ (1992) The Niquelândia mafic–ultramafic complex, Goiás, Brazil: a contribution to the ophiolite vs. stratiform controversy based on new geological and structural data. Precambrian Res 59:125–143

Ferreira Filho CF, Naldrett AJ, Gorton MP (1998). REE and pyroxene compositional variation across the Niquelândia layered intrusion, Brazil: petrological and metallogenetic implications. Applied Earth Science, Transactions of the Institutions of Mining and Metallurgy, Section B 107:1–21

Ferreira Filho CF, Araujo SM, Cruz HP (1999) Estruturas vulcânicas em granulitos da sequência vulcano-sedimentar Juscelândia, GO. Rev Bras Geosci 29:461–468

Ferreira Filho CS, Pimentel MM, Maria de Araujo S, Laux JH (2010) Layered intrusions and volcanic sequences in Central Brazil: geological and geochronological constraints for Mesoproterozoic (1.25 Ga) and Neoproterozoic (0.79 Ga) igneous associations. Precambrian Res 183:617–634

Figueiredo JA, Leao Neto R, Valente CR (1981). Depositos de sulfetos macros de Zn, Cu e Pb da região de Palmeirópolis, GO. In: SIMP GEOL CENTRO-OESTE, 1 Goiania, 1981 Ata, Goiania, SBG - Nucleos Centro-Oeste and Brasilia, pp 422–441.

Fugi MY (1989) REE geochemistry and Sm/Nd geochronology of the Cana Brava Complex, Brazil. Unpublishied Master Thesis, Kobe University, Japan, pp. 1–55

Giovanardi T, Girardi VAV, Correia CT, Sinigoi S, Tassinari CCG, Mazzucchelli M (2015) U-Pb zircons SHRIMP data from the Cana Brava Layered Complex: New constraints for the mafic-ultramafic intrusions of Northern Goiás, Brazil. Open Geosci 7:197–206

Girardi VAV, Kurat G (1982) Precambrian mafic and ultramafic rocks of the Cana Brava Complex, Brazil - mineral compositions and evolution. Rev Bras Geosci 12(1–3):313–323

Girardi VAV, Kawashita K, Basei MAS, Cordani U (1978) Algumas considerações sobre a evolução geológica da região de Cana Brava, a partir de dados geocronológicos. Congresso Brasileiro do Geologia, 1978, 30, Recife, Anais SBG 1:337–348

Girardi VAV, Rivalenti G, Sinigoi S (1986) The petrogenesis of Niquelandia layered basic–ultrabasic complex, central Goias, Brasil. J Petrol 27:715–744

Girardi VAV, Censi P, Comin-Chiaramonti P, Correia CT (1991) Análises isotópicas e difratométricas em dolomitas e grafitas de veios provenientes do Maciço de Cana Brava, Goiás. Anais do 3° Congresso Brasileiro de Geoquímica e 1° Congresso de Geoquímica dos Países de Língua Portuguesa. São Paulo, SP, Brasil, pp 583–585

Hofmann AW (1988) Chemical differentiation of the Earth: The relationship between mantle, continental crust and oceanic crust. Earth Planet Sc Lett 90:297–314

Holland T, Blundy J (1994) Non-ideal interactions in calcic amphiboles and their bearing on amphibole-plagioclase thermometry. Contrib Mineral Petrol 116:433–447

Junges SL, Pimentel MM, Moraes R (2002) Nd isotopic study of the Neoproterozoic Mara Rosa arc, Central Brazil: implications for the evolution of the Bras'ılia belt. Precambrian Res 117:101–118

Marangoni Y, Assumpcão M, Fernandes EP (1995) Gravimetria em Goiás, Brasil. Rev Bras Geosci 13:205–219

Matsui K, Girardi VAV, Basei MAS, Hasui Y (1976) Geocronologia do complexo básico-ultrabásico de cana Brava, Goiás. Congresso Brasileiro do Geologia, 1976, 29, Ouro Preto, Anais SBG 4: 279–288

Mazzucchelli M, Rivalenti G, Vannucci R, Bottazzi P, Ottolini L, Hofmann AW, Parenti M (1992) Primary positive Eu anomaly in clinopyroxenes of low-crust gabbroic rocks. Geochim Cosmochim Ac 56(6):2363–2370

Mercier JCC (1980) Single-pyroxene thermobarometry. Tectonophysics 70:1–37

Moore LJ, Murphy TJ, Barnes IL, Paulsen PJ (1982) Absolute Isotopic Abundance Ratios and Atomic Weight of a Reference Sample of Strontium. J of Res (NBS) 87(1):1–8

Moraes R, Fuck RA (1994) Deformação e metamorfismo das sequências Juscelândia e Serra da Malacacheta, Complexo Barro Alto. Goiás. Rev Bras Geosci 24:189–197

Moraes R, Fuck RA (1999) Trajetória P–T Horária para o Metamorfismo da Sequência Juscelândia, Goiás: Condições do Metamorfismo e Implicações Tectônicas. Rev Bras Geosci 29:603–612

Moraes R, Fuck RA (2000) Ultra-high-metamorphism in central Brasil: the Barro Alto complex. J Metamorph Geol 18:345–358

Moraes R, Fuck RA, Pimentel MM, Gioia SMCL, Figueiredo AMG (2003) Geochemistry and Sm–Nd isotope characteristics of bimodal volcanic rocks of Juscelândia, Goiás, Brazil: Mesoproterozoic transition from continental rift to ocean basin. Precambrian Res 125: 317–336

Moraes R, Fuck RA, Pimentel MM, Gioia SMCL, Hollanda MHBM, Armstrong R (2006) The bimodal rift-related volcanosedimentary sequence in Central Brazil: Mesoproterozoic extension and Neoproterozoic metamorphism. J S Am Earth Sci 20:287–301

Mori PE, Reeves S, Correia CT, Haukka M (1999) Development of a fused glass disc XRF facility and comparison with the pressed powder pellet technique at Instituto de Geociências. Rev Bras Geosci 29: 441–446

Navarro MS, Andrade S, Ulbrich HHGJ, Gomes CB, Girardi VAV (2008) The analysis of rare earth elements with ICP-MS in basaltic and related rocks: testing the efficiency of sample decomposition procedures. Geostand Geoanal Res 32(2):167–180

Pimentel MM, Fuck RA, Jost H, Ferreira Filho CF, Araujo SM (2000) The basement of the Brasília Fold Belt and the Goiás Magmatic Arc. In: Cordani UG, Milani EJ, Thomaz Filho A, Campos DA (eds) The Tectonic Evolution of South America, Rio de Janeiro Proceedings of the 31st International Geological Congress, Rio de Janeiro, pp 195–229

Pimentel MM, Ferreira Filho CF, Amstrong RA (2004a) Shrimp U–Pb and Sm–Nd ages of the Niquelandia layered complex: Meso (1, 25 Ga) and Neoproterozoic (0,79 Ga) extensional events in central Brasil. Precambrian Res 132:132–135

Pimentel MM, Jost H, Fuck RA (2004b) O embasamento da Faixa Brasilia e o Arco Magmático de Goiás. In: Geologia do

Continente Sul-Americano: Evolução da Obra de Fernando Flávio Marques de Almeida, pp 355–368

Pimentel MM, Ferreira Filho CF, Armele A (2006) Neoproterozoic age of the Niquelândia complex, Central Brazil: further ID-TIMS and Sm–Nd isotopic evidence. J S Am Earth Sci 21:228–238

Quick JE, Sinigoi S, Negrini L, Demarchi G, Mayer A (1992) Synmagmatic deformation in the underplated igneous complex of the IVZ. Geology 20:613–616

Quick JE, Sinigoi S, Mayer A (1994) Emplacement dynamics of a large mafic intrusion in the lower crust, Ivrea-Verbano zone, northern Italy. J Geophys Res 99(B11):21559–21573

Ribeiro Filho W, Teixeira NA (1981) Sequencia vulcano-sedimentar da Borda Oeste dos Complexos de Niquelandia e Cana Brava. Boletim informativo 10, SBG, Nucleo Centre-Oeste, pp 157–177

Rivalenti G, Girardi VAV, Sinigoi S, Rossi A, Siena S (1982) The Niquelandia mafic-ultramafic complex of central Goias, Brasil: petrological consideration. Rev Bras Geosci 12:380–391

Rivalenti G, Correia CT, Girardi VAV, Mazzuchelli M, Tassinari CC, Bertotto GW (2008) Sr–Nd isotopic evidence for crustal contamination in the Niquelandia complex, Goiàs, central Brasil. J S Am Earth Sci 25:298–312

Sato K, Tassinari CCG, Kawashita K, Petronilho L (1995) O método geocronológico Sm–Nd no IG/USP e suas aplicações. Annais, Brazilian. Acad Sci 67:313–336

Singer BS, Dungan MA, Layne GD (1995) Textures and Sr, Ba, Mg, Fe, K, and Ti compositional profiles in volcanic plagioclase: clues to the dynamics of calc-alkaline magma chambers. Am Mineral 80:776–798

Sisson TW, Grove TL (1993) Experimental investigations of the role of H_2O in calc-alkaline differentiation and subduction zone magmatism. Contrib Mineral Petrol 113:143–166

Suita MTF, Kamo S, Kroght TE, Fyfe WS, Hartmann LA (1994) U–Pb ages from the high-grade Barro Alto mafic–ultramafic complex (Goiás, central Brazil): middle Proterozoic continental mafic magmatism and upper Proterozoic continental collision. In: International Conference on Geochronology Cosmochronology and Isotope Geology, Berkeley, USGS, ICOG, Abstracts 8:309

Tanaka T, Togashi S, Kamioka H, Amakawa H, Kagami H, Hamamoto T, Yuhara M, Orihashi Y, Yoneda S, Shimizu H, Kunimaru T, Takahashi K, Yanagi T, Nakano T, Fujimaki H, Shinjo R, Asahara Y, Tanimizu M, Dragusanu C (2000) JNdi-1: a neodymium isotopic reference in consistency with LaJolla neodymium. Chem Geol 168:279–281

Thomas JB, Watson EB, Spear FS, Shemella PT, Nayak SK, Lanzirotti A (2010) TitaniQ under pressure: the effect of pressure and temperature on the solubility of Ti in quartz. Contrib Mineral Petrol 160: 743–759

Wells PR (1977) Pyroxene thermometry in simple and complex systems. Contrib Mineral Petrol 62:129–140

Workman RK, Hart SR (2005) Major and trace element composition of the depleted MORB mantle (DMM). Earth Planet Sc Lett 231:53–72